Nature Communications

https://doi.org/10.1038/s41467-026-70220-w

Article in Press

Targeting NAT10 alleviates colonic senescence and elderly-onset colitis by disrupting N4-acetylation of *DYRK1A*

Received: 12 February 2025

Accepted: 18 February 2026

Cite this article as: Chen, J., Xue, M., Mi, S. *et al.* Targeting NAT10 alleviates colonic senescence and elderly-onset colitis by disrupting N4-acetylation of *DYRK1A*. *Nat Commun* (2026). https://doi.org/10.1038/s41467-026-70220-w

Jingyu Chen, Meng Xue, Shuyi Mi, Anbo Fu, Wenwen Chen, Yuhao Sun, Shenglong Xia, Qiwei Ge, Jiakai Luo, Qiao Yu, Liangjing Wang & Shujie Chen

Targeting NAT10 Alleviates Colonic Senescence and Elderly-Onset Colitis by Disrupting N4-acetylation of *DYRK1A*

Jingyu Chen[1,2,3,4#], Meng Xue[1,2,3,#], Shuyi Mi[1,2,3,#], Anbo Fu[1,2,3], Wenwen Chen[1,2,3], Yuhao Sun[1,2,3], Shenglong Xia[1,2,3], Qiwei Ge[1,2,3], Jiakai Luo[1] , Qiao Yu[1], Liangjing Wang[1,2,3,*], Shujie Chen[2,3,5,*]

[1]Department of Gastroenterology, Second Affiliated Hospital of Zhejiang University School of Medicine, Hangzhou, Zhejiang, China

[2]Institution of Gastroenterology, Zhejiang University, Hangzhou, China

[3]Prevention and Treatment Research Center for Senescent Disease, Zhejiang University School of Medicine, Hangzhou, China

[4]Department of Gastroenterology, The Affiliated LiHuili Hospital of Ningbo University, Ningbo, China.

[5]Department of Gastroenterology, Sir Run Run Shaw Hospital, Zhejiang University School of Medicine, Hangzhou, Zhejiang, China

[#]These authors contributed equally: Jingyu Chen, Meng Xue, Shuyi Mi,

***Corresponding author:**

Shujie Chen, Sir Run Run Shaw Hospital, Zhejiang University School of Medicine, East Qingchun Rd, Hangzhou 310020, Zhejiang, PR China, Tel +86 0571 86006788, E-mail: chenshujie77@zju.edu.cn; **Liangjing Wang**, Second Affiliated Hospital of Zhejiang University School of Medicine, 88 Jiefang Rd, Hangzhou 310009, Zhejiang, PR China, Tel +86 0571 89713905, E-mail: wangljzju@zju.edu.cn;

Abstract

Intestinal aging characterized by imbalance between cell senescence and mucosal self-renewal, increases susceptibility to the elderly-onset ulcerative colitis (UC), while the underlying mechanisms remain elusive. Here, we identify mRNA N4-acetylcytidine (ac^4C) modification and its specific writer, N-acetyltransferase 10 (NAT10), as critical regulators of human colonic epithelial cell senescence. Knockdown of NAT10 significantly alleviates human colonic epithelial cell senescence *in vitro* and colonoid and intestinal aging *in vivo* in aged mice. Using ac^4C-modified transcriptome sequencing, we reveal that NAT10 stabilizes *DYRK1A* mRNA through ac^4C modification, thereby driving colon epithelial senescence. Moreover, NAT10 and DYRK1A are markedly upregulated in ulcerative colitis tissues from elderly patients and positively correlate with disease severity. Knockdown of NAT10, treatment with Nat10 or Dyrk1a inhibitor, alleviates colitis in aged mice. Collectively, these findings suggest that modulating NAT10-mediated RNA ac^4C modification could rejuvenate intestinal aging and provide a novel therapeutic strategy for elderly-onset colitis.

Introduction

Aging is characterized by progressive decline in organ physiology and cellular function, ultimately resulting in pathological alterations[1,2]. Aging-related intestinal changes include a thinner mucus layer, increased intestinal permeability, and impaired intestinal stem cell function[3-5]. Previous studies have demonstrated that aging-related intestinal deterioration contributes to the pathogenesis of colitis in aged rodents[6-10]. Consistently, recent epidemiological surveys reveal that ulcerative colitis (UC) exhibits a second incidence peak, with approximately 10% to 20% of cases occurring in individuals over 60 years old[11,12]. Treatment options for elderly UC patients are often constrained by comorbidities[13,14]. Additionally, elderly-onset UC patients frequently exhibit suboptimal responses to biologic therapies and face an increased risk of adverse reactions[15,16]. Beyond immunomodulators and biologic therapies, targeting intestinal aging represents a promising approach to mitigate elderly-onset UC[17].

Intestinal epithelial cells (IECs) form a critical barrier that protects the body from environmental toxins and pathogens[18]. Cell senescence, defined by the permanent halt in cell proliferation and defective apoptosis, is a cellular response to various sublethal endogenous and exogenous stresses[19]. Numerous factors have been implicated in driving cell senescence, including impaired DNA repair, mitochondrial dysfunction, disruption of protein homeostasis, and alterations in epigenetic regulation[20]. Epigenetic represents a reversible mechanism links genotype

to phenotype, which plays an important role in modulating the aging process in response to environmental stimulation[21]. Among them, RNA modifications represent an intriguing epitranscriptomic mechanism that fine-tunes gene expression, enabling rapid cellular responses and offering an energy-efficient means through the regulation of mRNA stability and translation. To date, over 170 types of RNA modifications have been identified, about 10 of which have been validated in mRNA within the mammalian transcriptome[22]. The ac^4C modification of mRNA has been shown to regulate RNA stability and translation efficiency[23]. Recent studies highlight the significance of mRNA ac^4C modifications in various biological processes, such as growth, development, and tumorigenesis[24-26]. However, the roles of mRNA ac^4C modification in regulating cell senescence and age-related diseases remain largely unexplored.

Here, we reported a significant upregulation of mRNA ac^4C modification and its unique known writer N-acetyltransferase 10 (NAT10), and uncovered their roles on colon epithelial cell senescence. NAT10 stabilizes *DYRK1A* mRNA, thereby promoting colon epithelial cell senescence in an RNA ac^4C-dependent manner. Notably, Nat10/Dyrk1a axis plays a critical role in colonic senescence**,** and provides therapeutic targets to mitigate colitis in aged mice. Clinically, NAT10 and DYRK1A are upregulated in ulcerative colitis tissues from elderly patients, and related with more severe disease status. Collectively, these findings suggest that targeting NAT10-mediated RNA ac^4C modification may rejuvenate colonic cell senescence and alleviate the elderly-onset UC.

Results

mRNA ac^{4}C modification and its writer NAT10 are upregulated in the senescent colon epithelial cells

We establish H_2O_2- (H-Sen) or Doxorubicin- (D-Sen) induced cell senescence models in the immortalized colon epithelial cell line NCM460 and the diploid finite colon epithelial cell line CCD841. We then utilized LC-MS/MS to detect the mRNA modification from both above senescent and proliferative cells **(Figure. 1a)**. The senescent state of the cells was confirmed by SA-Gal staining **(Figure. 1b),** G1 cell-cycle arrest **(Supplementary Figure. 1a,b)** and the upregulation of classical pro-inflammatory senescence-associated secretory phenotype (SASP) genes (*IL-1β* and *IL-6*) **(Supplementary Figure. 1c,d)**. The ac^{4}C modification of mRNA was consistently upregulated in both H-Sen and D-Sen induced senescent NCM460 and CCD841 cell lines **(Figure. 1c,d)**. N-acetyltransferase 10 (NAT10), the specific writer of mRNA ac^{4}C modification, were upregulated in senescent colon epithelial cells, accompanied by increased expression level of aging-related markers (p53, p21, p16 and γ-H2AX) and reduced expression of the cell-cycle regulator Cyclin D1 **(Figure. 1e)**. We next established a replicative senescence model when passage 20 in CCD841 cells, characterized by an enlarged and flattened morphology

and increased proportion of SA-Gal positive cells **(Figure. 1f and Supplementary Figure. 1e,f)**. Similarly, the RNA ac^4C modification and NAT10 protein levels was significantly upregulated in replicative-senescent CCD841 cells **(Figure. 1g and Supplementary Figure. 1g)**.

NAT10 regulates colon epithelial cell senescence through mRNA ac^4C modification

We then explore whether NAT10 regulates the senescence of colon epithelial cells in an RNA ac^4C modification-dependent manner. Results showed that overexpression of wild type NAT10 (NAT10-WT) increased mRNA ac^4C modification which was impaired by NAT10 knockdown **(Supplementary Figure. 2a,b)**, whereas overexpression of mutant plasmid (NAT10-MUT) failed **(Figure. 2a)**. Overexpression of NAT10-WT, while not NAT10-MUT, could partially reverse the downregulation of aging-related markers (p53, p21, p16 and γ-H2AX) and the percentages of SA-Gal and γ-H2AX positive cells, as well as upregulation of Cyclin D1 and the positive percentage of EdU under H_2O_2 or DOX treatment condition **(Figure. 2b,c and Supplementary Figure. 2c-e)**.

Resistance to apoptosis is a hallmark feature of cellular senescence[27]. We next investigated the role of NAT10 in the senescent cell viability **(Figure. 2d)**. A significant decrease number of colonies formation was observed in senescent colonic epithelial cells following 48 hours of *NAT10* siRNA transfection. Overexpression of NAT10-WT, while not NAT10-MUT, increased the number of colonies in both H-Sen and D-Sen cells **(Figure. 2e and Supplementary Figure. 2f)**. In addition, NAT10 knockdown reduced cell viability, but increased caspase 3/7 apoptotic activity in senescent cells. Reintroduction of NAT10-WT could rescue this phenotype **(Figure. 2f,g and**

Supplementary Figure. 2g,h). Apoptosis assays further confirmed that NAT10 maintained the resistance of senescent cells to apoptosis in an RNA ac^4C-dependent manner. **(Figure. 2h and Supplementary Figure. 2i)**.

Knockdown Nat10 alleviates intestinal aging in mice

Previous findings on senescent colonic cells prompted us to further explore the expression of Nat10 in the colon of mice at different ages. Nat10 is predominantly localized in the colonic epithelial crypts, and its protein expression levels progressively increased in the colonic tissues in mice from 2, 6, 12, to18 months old **(Figure. 3a,b)**. Accordingly, RNA ac^4C modifications and the expression of *Il-1β, Il-6*, and *TNF-α* were upregulated in the intestines of 18-mon mice compared to those of 2-mon mice **(Supplementary Figure. 3a,b)**.

To investigate the role of Nat10 in colons, Littermate $Nat10^{+/-}$ and Nat10-WT mice were co-housed, and colonic cell senescence was assessed in aged mice **(Figure. 3c)**. In colonic tissues from Aged-$Nat10^{+/-}$ mice, Nat10 protein expression levels were significantly lower compared to Aged-WT mice. As marker of cell senescence, the expressions of p16, p21 and p53 were decreased, while Lgr5 and Ocln were upregulated in Aged-$Nat10^{+/-}$ mice **(Figure. 3d)**. Furthermore, the colonic mucosal height and the fluorescence intensity of Ocln as well as the number of Ki67-positive and goblet cells ($Muc2^+$) were increased in Aged-$Nat10^{+/-}$ while the number of γ-$H2AX^+$ diminished **(Figure. 3e and Supplementary Figure. 3c)**. Additionally, qPCR analysis showed that the expression of *Il-1β, Il-6*, and *TNF-α* in colonic tissues were significantly downregulated in Aged-$Nat10^{+/-}$ mice **(Supplementary Figure. 3d)**. Similarly, knockdown of Nat10 via AAV-

shNat10 delivery system in aged mice also resulted in decreased expression of p16 and p21**(Figure. 3f)**, accompanied by increased expression of Ocln and $Ki67^{+}$ in epithelial cells **(Figure. 3g and Supplementary Figure. 3e)**. Collectively, these findings indicate that lowering NAT10 protein levels can diminish senescent cell accumulation and rejuvenate colon stem cells, thus enhancing mucosal barrier regeneration.

To further substantiate the role of NAT10 in intestinal aging, we intraperitoneally injected with a NAT10 inhibitor Remodelin, to aged mice every three days for two months **(Supplementary Figure. 4a)**. Biomarker of *p53* and *p21* were significantly downregulated in colon tissues when treated with Remodelin **(Supplementary Figure. 4b)**. A significant increase in colon mucosal height, goblet cells and Ki67 positive cells in crypts, as well as the fluorescence intensity of the Ocln was observed **(Supplementary Figure. 4c,d)**. In addition, Remodelin exhibited well tolerability in aged mice, without significant alterations in serum biochemical parameters or histopathological change in major organs (heart, liver, spleen, lung, and kidney) **(Supplementary Figure. 4e,f)**.

DYRK1A as a target gene of NAT10-mediated RNA ac^4C modification

To further explore candidate target genes with ac^4C modification, we performed acRIP-seq on senescent colon epithelial cell knockdown of NAT10 or not, as well as wild type NCM460 cells **(Figure. 4a)**. A summary of peak numbers and ac^4C-enriched gene counts for each sample is presented in the **Supplementary Table 1.** We observed that ac^4C modifications on mRNA were

enriched in CDS region **(Figure. 4b and Supplementary Figure. 5a)**. Motif analysis showed that ac^4C modifications were highly enriched within a C-rich sequence, which is consistent with previously reported results[28] **(Supplementary Figure. 5b)**. 1,228 hyperacetylated peaks ($log_2FC > 0$) corresponding to 858 genes were identified in the H-Sen group compared with the control group. In contrast, 640 hypoacetylated peaks ($log_2FC<0$) corresponding to 529 genes were detected in the H-Sen NAT10-Si group. GO enrichment analysis of hyperacetylated genes in senescent NCM460 cells revealed that these transcripts were functionally enriched in several senescence-related biological processes, including autophagy, type I interferon signaling, and DNA damage signaling[27,29,30]. While hypoacetylated genes in senescent NCM460 cells with NAT10 knockdown showed that these genes were primarily involved in the transmission and regulation of DNA damage response signaling pathways **(Figure. 4c)**.

To identify the potential targets through which NAT10-mediated RNA ac^4C modification, we first identified 32 protein-coding transcripts that exhibited increased ac^4C abundance ($|log_2FC|>1.5$) in H-Sen. Upon NAT10 knockdown in H-Sen (H-Sen-Si vs. H-Sen), 11 protein-coding transcripts showed reduced ac^4C abundance ($|log_2FC|>1.5$). We intersected the differentially acetylated transcripts and identified four candidate genes: *THAP5, DYRK1A, LMLN*, and *MVB12A* **(Figure. 4d)**. acRIP-qPCR confirmed that ac^4C enrichment on *DYRK1A* and *LMLN* were consistent with the sequencing data **(Figure. 4e)**. In line with this, qPCR analyses indicated that only *DYRK1A* mRNA showed consistent changes **(Figure. 4f)**. It has been reported that NAT10 enhances mRNA acetylation, which subsequently increases mRNA stability and translation[23,31]. To further validate

this, we performed RNA sequencing followed by transcription inhibitor actinomycin D (Act-D) treatment, and found that only *DYRK1A* mRNA, among the candidates (*THAP5, DYRK1A, LMLN*, and *MVB12A*), was regulated by NAT10, with its expression decreasing over time **(Figure. 4g and Supplementary Figure. 5c)**. Consistently, merged IGV visualization for three groups of our acRIP-seq data revealed multiple changes in ac^4C modifications across the CDS region of *DYRK1A* mRNA **(Figure. 4h and Supplementary Figure. 5d)**. Western blot analysis further confirmed that NAT10 regulates DYRK1A protein expression **(Figure. 4i)**. Collectively, these findings suggest that *DYRK1A* is a critical downstream effector of ac^4C-mediated cellular senescence in colonic epithelial cells.

NAT10 promotes colon epithelial cell senescence by regulating *DYRK1A* mRNA stabilization

We observed significant enrichment of ac^4C modification on the CDS domain of *DYRK1A* transcripts in senescent NCM460 cells **(Figure. 5a)**. Additionally, the RNA and protein expression levels of DYRK1A were increased in senescent colon epithelial cells **(Figure. 5b)**. Further immunofluorescence analysis confirmed that DYRK1A expression was relatively elevated in senescent cells, accompanied with higher DNA damage marker γ-H2AX **(Figure. 5c)**. We hypothesized that NAT10-mediated ac^4C modification directly regulates DYRK1A expression. We performed NAT10-RIP qPCR assay and observed an increased binding between NAT10 protein and CDS domain of *DYRK1A* RNA in senescent cells **(Figure. 5d)**. To further investigate whether

transcriptional regulation of *DYRK1A* by NAT10 in senescent cells, the *DYRK1A* promoter was cloned into a luciferase reporter plasmid. No significant change in luciferase activity of the *DYRK1A* promoter was observed after knocking down NAT10 in senescent cells **(Supplementary Figure. 5d)**.

It has been reported that NAT10 enhances mRNA acetylation, which subsequently increases mRNA stability and translation[23,31]. We assumed that the increased expression of DYRK1A might be due to post-transcriptional regulation. To validate this, NCM460 cells were treated with the actinomycin D (Act-D). We observed that *DYRK1A* mRNA stability was increased in senescent cells. However, upon NAT10 knockdown in senescent colon epithelial cells, *DYRK1A* mRNA stability was reduced **(Figure. 5e)**. Previous studies have shown that ac4C modification within the CDS region can regulate not only mRNA stability but also its translational efficiency. In line with this, polysome profiling followed by qPCR quantification demonstrated a reduced association of *DYRK1A* mRNA with heavy polysomes upon NAT10 knockdown, supporting that NAT10-mediated ac^{4}C modification also promotes DYRK1A translation **(Figure. 5f)**.

We next confirmed that overexpression of DYRK1A could rescue the senescence reduction effect induced by NAT10 knockdown (**Figure. 5g**), along with downregulation of *IL-1β* and *IL-6* mRNA expressions (**Figure. 5h**), γ-H2AX, p21 protein expressions (**Figure. 5i**), and upregulation of caspase3/7 activity in senescent cells (**Figure. 5j**).

A significant upregulation of *DYRK1A* mRNA and protein was observed in replicative senescent colon epithelial CCD841 cells **(Supplementary Figure. 6a)**. Additionally, acRIP-qPCR

and RNA decay assays corroborated that the ac^4C modification on CDS domain of *DYRK1A* mRNA was enriched, accompanied by increased mRNA stability in replicative senescent colon epithelial cells **(Supplementary Figure. 6b,c)**. We then knocked down DYRK1A in passage 15 CCD841 cells and observed a marked increase in EdU^+ proliferating cells **(Supplementary Figure. 6e)** ,and a reduction in SA-Gal^+ senescent cells **(Supplementary Figure. 6f)**, further supporting the role of DYRK1A in promoting colonic epithelial senescence. Moreover, overexpression of DYRK1A could rescue the reduction in the senescence phenotype caused by NAT10 knockdown in CCD841 cells **(Supplementary Figure. 6g,h)**.

Targeting NAT10/DYRK1A axis delays colon senescence in mice.

We treated aged mice with the DYRK1A inhibitor Harmine (10 mg/kg, intraperitoneally, every three days for two months) **(Supplementary Figure. 7a)**. Notably, Harmine treatment led to a significant increase in $Ki67^+$ epithelial cells in colonic crypts **(Supplementary Figure. 7b),** suggesting enhanced epithelial regenerative capacity. In addition, Harmine exhibited well tolerability in aged mice, without significant changes in serum biochemistry or histopathology of key organs **(Supplementary Figure. 7c,d).**

To further determine the functional relevance of the NAT10/DYRK1A axis in regulating colonic aging, we next performed AAV-mediated gene manipulation in aged mice. Knockdown of Nat10 via AAV-shNat10 delivery system significantly alleviated colonic senescence, as evidenced by improved epithelial morphology and reduced expression of p16 and p21. Re-expression of

DYRK1A (AAV-Dyrk1a) reversed these protective effects, restoring colonic senescence as comparable to control group **(Supplementary Figure. 7e,f).**

NAT10 knockdown or pharmacological inhibitor treatment in aged mice promotes intestinal organoid regeneration *in vivo*

We and others have demonstrated that impaired intestinal epithelial regenerative capacity in intestinal organoids is a key characteristic of cell senescence[32-34]. We then isolated colonoids from Young-WT and Aged-WT mice, as well as Aged-Nat10$^{+/-}$ mice **(Figure. 6a)**. Results revealed that colonoids derived from Aged-Nat10$^{+/-}$ mice exhibited superior stemness and proliferative capabilities compared to those from Aged-WT mice. Specifically, Aged-Nat10$^{+/-}$ colonoid displayed a higher proportion of budding, increased EdU level **(Figure. 6b)**, faster budding growth rate **(Figure. 6c)**, and elevated expression of Lgr5 protein **(Figure. 6d)**. Additionally, the enhanced proliferation and differentiation capacities of Aged-Nat10$^{+/-}$ colonoid were further validated by the downregulation of *p21* and the upregulation of *Pcna* and *Muc2* **(Figure. 6e,f)**. Remodelin was administrated every three days into aged mice for two months and colonoids were isolated **(Supplementary Figure. 8a)**. We found an increased proportion of budding colonoid **(Supplementary Figure. 8b)** and Lgr5 protein expression **(Supplementary Figure. 8c)**. Enhanced proliferation and differentiation capacities were also observed in the Remodelin treatment group **(Supplementary Figure. 8d,e)**. Taken together, these results indicate that deletion with Nat10 enhances cell stemness and proliferation capacity in colonoid from aged mice.

Previous studies have reported that in colonoids, LPS can increase ER stress, leading to DNA damage and reduced proliferation capacity [35]. We validated the appropriate LPS concentration for Aged-WT colonoid in an *in vitro* model **(Supplementary Figure. 8f)**. After treating with complete culture medium containing 5μg/ml LPS **(Figure. 6g)**, we found that Aged-Nat10$^{+/-}$ mice or Remodelin-treated Aged-WT colonoids maintained relatively higher levels of *Lgr5* mRNA **(Figure. 6h)**, and a higher proportion of budding colonoid **(Figure. 6i,j)**. Aged-Nat10$^{+/-}$ or Remodelin-treated Aged-WT colonoids exhibited a reduction of γ-H2AX and Dyrk1a **(Figure. 6k)**.

Targeting the NAT10/DYRK1A axis alleviates colitis in aged mice

Intestinal aging aggravates the susceptibility and severity of ulcerative colitis[6,17]. We further investigated the impact of intraperitoneal injection of NAT10 inhibitor Remodelin on DSS-induced colitis in Aged-WT mice **(Supplementary Figure. 9a)**. Interestingly, Remodelin treatment markedly reduced body weight loss in aged mice **(Supplementary Figure. 9b)**. Results revealed that a decrease in ac^{4}C modification levels in Aged-WT mice following Remodelin treatment in colon tissues **(Supplementary Figure. 9c).** The Remodelin-treated group exhibited significantly reduced histopathological damage and the number of γ-H2AX-positive cells in Aged-WT mice **(Supplementary Figure. 9d)**. Additionally, we observed a downregulation of Dyrk1a protein level following Remodelin treatment in colitis mice **(Supplementary Figure. 9e)**.

To confirm the role of NAT10 in aged colitis, we then treated Aged-Nat10-WT or Nat10$^{+/-}$ littermate mice with DSS-containing water for 7 days **(Figure. 7a)**. Compared to Nat10-WT mice,

Aged-Nat10$^{+/-}$ mice showed significantly reduced body weight loss **(Figure. 7b)**, colon shortening **(Figure. 7c)**, as well as lower colonoscopy score and histopathological score **(Figure. 7d,e)**. Correspondingly, RNA ac^{4}C levels were decreased in the colons of Aged- Nat10$^{+/-}$ mice **(Figure. 7f)**. Based on these results, we hypothesized that upregulation of Nat10 may exacerbate colitis in aged mice, and depletion with Nat10 protein could alleviate DSS-induced colitis. Results confirmed a relative reduction in the number of γ-H2AX-positive cells, along with significant increase in Ki67-positive cells, goblet cells **(Figure. 7g,h)**. The mRNA levels of *p21* and intestinal inflammatory genes (*Il-1β, Il-6*, and *Tnf-α*) were significantly reduced in the colonic tissues of Aged-NAT10$^{+/-}$ mice **(Figure. 7i)**. Additionally, Dyrk1a and γ-H2AX protein levels were decreased, while the barrier protein Ocln was upregulated **(Figure. 7j,k)**. These findings further prompted us to investigate the role of Dyrk1a in colitis. We then used Harmine, a well-established Dyrk1a inhibitor, to treat aged mice in colitis model followed by colonoscopic examination **(Supplementary Figure. 9f)**. Enema treatment with Harmine (10mg/kg) for 3 days significantly promoted the healing of colonic mucosal ulcers compared to Vehicle control group **(Supplementary Figure. 9g)**.

To further determine the role of NAT10/DYRK1A axis in elderly-onset colitis, we performed AAV-mediated gene manipulation in aged mice **(Figure. 7l)**. Knockdown of Nat10 via AAV-shNat10 significantly alleviated DSS-induced colitis, as reflected by reduced body weight loss and lower histopathological scores. Re-expression of DYRK1A (AAV-Dyrk1a) reversed these protective effects, restoring colitis severity **(Figure. 7m,n)**. These findings further support that

targeting the NAT10/DYRK1A axis play a critical role in mitigating colitis in aged mice.

NAT10 and DYRK1A highly expressed in the aged colon and elderly UC tissues.

Immunohistochemical analysis of colon biopsy samples in our clinical cohort further confirmed the upregulation of NAT10 and DYRK1A in the colonic mucosa of healthy elderly individuals as well as elderly-onset UC patients **(Figure. 8a-c).** In addition, a positive correlation between NAT10 and DYRK1A immunohistochemical scores was observed in UC biopsy samples **(Figure. 8d)**. Moreover, NAT10 and DYRK1A expression levels were higher in colonic mucosa from elderly UC patients with high endoscopic Mayo scores compared with those with low scores **(Figure. 8e)**. Collectively, these findings suggest that the NAT10/DYRK1A axis may hold translational relevance and represent a potential therapeutic target for elderly-onset colitis.

Discussion

In this study, we identified mRNA ac^4C modification and its specific writer N-acetyltransferase 10 (NAT10) are upregulated in senescent colon epithelial cells. NAT10 modulates colon epithelial cell senescence by stabilizing *DYRK1A* mRNA in an RNA ac^4C-dependent manner. Nat10 kncokdown or treatment with its inhibitor Remodelin significantly alleviated DSS-induced colitis in aged mice. Emerging evidence indicate that ac^4C modification of mRNA is involved in the progression of various human diseases, including cancers, osteoporosis,

and autoimmune disorders such as rheumatoid arthritis and systemic lupus erythematosus (SLE)[31,36-39]. A preclinical study shows that targeting NAT10 *in vivo* significantly enhances the healthspan in a $Lmna^{G609G}$ Hutchinson-Gilford Progeria Syndrome (HGPS) mouse model[40]. However, the regulatory mechanisms by which NAT10 influences aging and age-related diseases remain poorly understood.

DYRK1A mRNA was identified as a direct target of NAT10-mediated RNA ac^4C modification. DYRK1A, a member of the DYRK family, is characterized by its dual ability to autophosphorylate tyrosine residues and phosphorylate serine/threonine residues in substrate proteins, and also involved in various biological processes, including cell cycle regulation, cell signaling transduction, and cell senescence[41,42]. In cell cycle regulation, DYRK1A phosphorylates key substrates, such as p53, $p27^{Kip1}$, and Cyclin D1. For example, it phosphorylates P53 at Ser15, inducing cell cycle arrest in embryonic neuronal cells[43-45]. In cell signaling transduction, DYRK1A phosphorylates STAT3 at Ser727, a conserved site essential for its function in both humans and mice[46,47]. Recent study suggests that DYRK1A overexpression may accelerate cell senescence, particularly in Down syndrome (DS), by exacerbating laminopathy through Lamin B1 downregulation[48]. In this study, overexpression of DYRK1A was found to exacerbate the senescence phenotypes in colon epithelial cells and colonic aging *in vivo*. NAT10 enhances *DYRK1A* mRNA stability through ac^4C RNA acetylation, sustaining DYRK1A protein expression in senescent colon epithelial cells. The specific ac^4C location on *DYRK1A* mRNA is not pinpointed, and further investigation into the deposition of the ac^4C site is necessary. In addition, several

transcription factors, including REST[49] and MEF2D[50], have been reported to regulate *DYRK1A* expression in different cellular contexts. Incorporating these factors as biological positive controls would further strengthen the conclusions derived from our transcriptional reporter assays in future.

Studies have reported that reducing cellular senescence can alleviate experimental UC. For example, study demonstrated that the senolytic combination of Dasatinib and Quercetin significantly alleviate intestinal senescence and inflammation in aged mice[8,51-53]. Senescent cells trigger DNA damage responses that increase the release of pro-inflammatory cytokines, worsening age-related inflammation[54]. Recent studies have highlighted DYRK1A's involvement in DNA damage response. Reducing DYRK1A expression or using its inhibitors led to decreased γ-H2AX foci per nucleus[48]. In our study, Nat10 knocdown and its specific inhibition by Remodelin reduced DNA damage and promoted colonic epithelial proliferation in both aged colitis mice and colonoid models. Several studies have demonstrated that enhanced epithelial proliferation promotes epithelial regeneration, attenuates mucosal injury, and improves recovery following inflammation or epithelial damage[55-57]. In addition, NAT10 and DYRK1A expression levels were elevated in ulcerative colitis tissues from elderly patients, and their expression positively correlated with disease severity. These results suggest that the NAT10/DYRK1A axis may serve as potential therapeutic targets for elderly-onset UC.

In summary, the mRNA ac^4C modification and its specific writer N-acetyltransferase 10 (NAT10) are characterized as key regulators in senescent colon epithelial cells. Reducing NAT10-mediated ac^4C modification alleviated colon epithelial cell senescence by regulation *DYRK1A*

mRNA stability. Upregulation of NAT10 was positively correlated to DYRK1A in elderly-onset UC patients, which suggest that NAT10-mediated ac^4C modification is crucial for colonic cell senescence and provide a novel therapeutic approach for elderly-onset UC.

Methods

Cell culture

The colon epithelial cell line NCM460 (Cellosaurus, #305430, RRID: CVCL_0460) was cultured in RPMI 1640 medium (GIBCO, Waltham, MA, USA), and the finite colon cell line CCD841 (ATCC, CRL-1790, RRID: CVCL_2871) was maintained in Eagle's minimum essential medium (ATCC, Manassas, VA, USA). Each medium was supplemented with 10% fetal bovine serum (ExCell Bio, Suzhou, China) and 1% penicillin-streptomycin (Beyotime, Shanghai, China). All cells were incubated at 37°C in a humidified atmosphere with 5% CO2.

Cell senescence induction

To induce replicative senescence, we performed consecutive passages of CCD841 cells. To induce senescence using Doxorubicin (DOX) (Sigma Aldrich, St. Louis, MO, USA), NCM460 or CCD841 cells were cultured in the presence of DOX (300 nM) in complete culture media for 72 h. Cells were maintained for an additional 5 days after DOX withdrawal before senescence assays were conducted.

For the H_2O_2-induced senescence model (H-Sen), we adapted protocols for colorectal cancer cell

lines[58], human fibroblasts[59] and optimized the conditions accordingly. In brief, NCM460 cells were first exposed to 250 μM H_2O_2 for 48 hours, followed by incubation in medium containing 50 μM H_2O_2 for an additional 6 days to establish a stable senescent phenotype. The H_2O_2-containing medium was replaced daily throughout the induction period.

SA-Gal staining

SA-Gal activity was assessed using a SA-Gal staining kit (Beyotime, Shanghai, China). In brief, cells were rinsed three times with phosphate-buffered saline (PBS) and fixed at room temperature (RT) for 15 minutes with the fixing solution included in the SA-Gal staining kit. After being washed three more times with PBS, the cells were incubated overnight at 37°C in senescence detection solution. The stained cells were subsequently examined under a light microscope.

Cell Cycle Analysis

Cell cycle distribution was analyzed by propidium iodide (PI) staining followed by flow cytometry. Briefly, cells were collected and fixed in 70% ice-cold ethanol at −20°C for at least 2 h. After washing with PBS, cells were incubated with RNase A (100 μg/mL) and PI (50 μg/mL) for 30 min at room temperature in the dark. Samples were analyzed on a flow cytometer and processed using FlowJo software.

Luciferase reporter assay

DYRK1A promoter region ((−2000 to +100 bp) relative to the transcription start site) into the

pGL4.10 firefly luciferase vector. The Renilla luciferase plasmid pRL-TK was co-transfected for normalization. The dual-luciferase reporter assay was conducted using the Dual-Luciferase Reporter Assay System (Vazyme, DD1205, China). Cells were plated in 6-well plates and transfected with Lipofectamine 3000. CMV-driven firefly luciferase plasmid was included as a positive control. After 24 hours of transfection, Firefly and Renilla luciferase activities were measured according to the manufacturer's instructions. Firefly luciferase activities were normalized to Renilla luciferase activities, and the ratio of Firefly to Renilla luminescence was calculated.

EdU assay

EdU incorporation was assessed using the EdU Imaging Kit (APEXBIO, K1076, USA) following the manufacturer's instructions. Cells were exposed to 10 μM EdU for 1 hour, harvested by trypsinization, and washed with PBS. They were then fixed with 4% paraformaldehyde for 20 minutes and permeabilized in 0.1% Triton X-100 for 20 minutes. After two additional PBS washes, single-cell suspensions were incubated with the EdU detection reagent for 30 minutes at room temperature in the dark. Samples were analyzed on a flow cytometer and processed using FlowJo software.

Quantitative PCR

Total RNA was extracted from cells or tissues using TRIzol reagent (Invitrogen, Carlsbad, CA, USA). A magnetic mRNA isolation kit (NEB, Ipswich, MA, USA) was utilized to isolate poly

(A)+ mRNA from total RNA. Quantitative PCR (qPCR) was carried out with ChamQ Universal SYBR qPCR Master Mix (Vazyme, Nanjing, China,) on a Light Cycler 480 II system (Roche, Basel, Switzerland). Reactions were performed in triplicate, and β-actin was used for mRNA normalization. Primer sequences for qPCR are listed in **Supplementary Table 2**. The $2^{-\Delta\Delta Ct}$ method was employed to determine relative mRNA expression levels.

Liquid chromatography-tandem mass spectrometry for RNA modification dection

A magnetic mRNA isolation kit (NEB, Ipswich, MA, USA) was used to isolate poly (A)+ mRNA from total RNA. The isolated mRNA (200 ng) was digested into nucleosides using 0.5 U nuclease P1 (FUJIFILM Wako, Tokyo, Japan) in 20 μL of buffer containing 10 mM ammonium acetate, pH 5.3, at 42 °C for 6 hours. Subsequently, 2.5 μL of 0.5 M MES buffer, pH 6.5, and 0.5 μL shrimp alkaline phosphatase (NEB, USA) were added, followed by incubation at 37 °C for an additional 6 hours. The mixture was then analyzed using liquid chromatography-tandem mass spectrometry (LC-MS/MS). Nucleosides were separated using ultra-performance liquid chromatography on a C18 column and detected by a triple-quadrupole mass spectrometer (AB SCIEX QTRAP 5500) in positive-ion multiple reaction monitoring mode. Mass transitions at m/z were monitored and compared to standard samples (Zz Standard, Shanghai, China), and nucleoside concentrations in the RNA samples were quantified by matching signal intensities to standard curves.

Plasmid and lentivirus construction

Full-length NAT10-WT, NAT10-K290A and DYRK1A was amplified and cloned into a pLVX-

puro plasmid. HEK 293 T cells were transfected with above mentioned plasmids and the virus packing plasmids using PolyJet transfection reagent (SignaGen, Rockville, MD, USA). The viral supernatants were harvested and enriched via centrifugation.

SiRNAs construction and transfection

For transient knockdown, siRNAs targeting the *NAT10* mRNA and *DYRK1A* mRNA were purchased from GenePharma (Shanghai, China). siRNA duplexes were transfected using Lipofectamine RNAiMAX (Invitrogen, Carlsbad, CA, USA)). Transfection was performed according to the manufacturer's instructions. The siRNA sequences used in this study are listed in **Supplementary Table 3.**

RNA immunoprecipitation-qPCR

Cells were lysed using RNA immunoprecipitation (RIP) buffer (25 mM Tris, pH 7.4, 150 mM KCl, 0.5 mM DTT, and 0.5% NP-40) supplemented with RNase inhibitors (1:500, Beyotime, Shanghai, China). NAT10 antibodies (2 μg, Abcam, Cambridge, UK) or the anti-IgG (2 μg, Beyotime, Shanghai, China) were added to the RIP buffer and incubated overnight at 4 °C. Then, Protein A/G magnetic beads were added to the mixture and incubated for 4 h at 4 °C, followed by washing three times with NT2 buffer (50 mM Tris, pH 7.4, 150 mM NaCl, 1 mM MgCl2, 0.05% NP-40). Input and immunoprecipitated RNAs were isolated using TRIzol, followed by qRT-PCR.

Acetylated RIP-seq

Total RNA was extracted using the previously described method and then heated to 70 °C for 6

minutes. The reaction was halted by the addition of EDTA. The fragmented RNA was subsequently purified using the Zymo RNA Clean and Concentrator-25 kit (R1017; Zymo Research, Costa Mesa, CA, USA). The purified RNA was incubated with an anti-ac^{4}C antibody and Dynabeads Protein G (10004D; Invitrogen, Carlsbad, CA, USA)) at 4 °C for 6 hours. Following the manufacturer's guidelines, the immunoprecipitated RNA was collected. Library construction was performed with the EpiTM Mini LongRNA-seq Kit (E1802; Epibiotek) in accordance with the provided protocol. Library quality was assessed using a Bioptic Qsep100 Analyzer (Bioptic). Sequencing was carried out on the NovaSeq high-throughput platform by Epibiotek (Guangzhou, China).

Acetylated RIP-qPCR assay

The ac^{4}C modifications in individual genes were determined using acetylated (ac)RIP-qPCR assay. Briefly, cells cultured in a 10-cm plate were washed three times with ice-cold PBS and harvested by scraping in 1 mL of RIP buffer supplemented with RNase inhibitors. The TRIzol reagent was used for total RNA isolation. One-tenth of the total RNA was used as the input. Then, 80 μg of total RNA and 2 μg of ac^{4}C antibody were added to RIP buffer supplemented with RNase inhibitors (1:500) and incubated overnight at 4 °C. Then, prewashed Protein A/G magnetic beads were added to the mixture and incubated for 4 h. Following five washes, the acetylated RNA was eluted from the magnetic beads using TRIzol. Eluted RNAs were precipitated using ethanol and dissolved in RNase-free water. The enrichment of certain fragments was detected using qPCR. The proportion of ac^{4}C-enriched RNA to input RNA is presented as the ac^{4}C level.

Western blotting

Total protein was extracted using RIPA lysis buffer supplemented with protease inhibitors. The samples were separated by sodium dodecyl sulfate-polyacrylamide gel electrophoresis (SDS-PAGE) and transferred onto a polyvinylidene fluoride (PVDF) membrane. After blocking with 5% bovine serum albumin (BSA) for 2 hours at room temperature (RT), the membranes were incubated overnight at 4°C with the following primary antibodies: NAT10 (1:1000, Abcam, ab194297, UK), p53 (1:1000, 10442-1-AP,Proteintech, Rosemont, IL, USA), p21 (1:1000, 10355-1-AP and 28248-1-AP, Proteintech, USA), p16 (1:1000, Proteintech, 10883-1-AP and 28416-1-AP USA), Occludin (1:1000, Proteintech, 27260-1-AP, USA), Cyclin D1 (1:1000, CST, #2978, USA), γ-H2AX (1:1000, ABclonal Technology, AP0687, MA, USA), DYRK1A(1:1000, Bioss, bs-11834R, China), LMLN(1:1000, Bioss, bs-18180R, China), THAP5 (1:500, OriGene, Rockville, MD, USA), Lgr5 (1:1000, Bioss, bs-20747R, China) and β-actin (loading control) (1:1000, CST, #4967, Danvers, MA, USA). Universal antibody diluent (NCM Biotech, Suzhou, China) was used for antibody dilution. The membranes were then washed three times with Tris-buffered saline containing Tween 20 (TBST) and incubated with horseradish peroxidase-conjugated secondary antibody (1:5000, Beyotime, Shanghai, China). Protein signals were detected using the ECL Western Blot Substrate (NCM Biotech, Suzhou, China) and visualized on an Azure 600 Gel Imaging System (1.6.3.1211, Azure Biosystems, Dublin, CA, USA)

RNA ac^{4}C dot blot assay

A total of 2μl containing 1 μg of RNA was heated to 65 °C for 5 minutes and subsequently

transferred onto a Hybond-N+ membrane (GE Healthcare, Wauwatosa, WI, USA). The membranes were UV crosslinked for 30 minutes and stained with 0.02% methylene blue (Sangon Biotech, Shanghai, China) to visualize the input RNA. After blocking with 5% BSA, the membranes were incubated overnight at 4°C with an ac^4C-specific antibody (diluted 1:250, Abcam, UK). Following three washes with TBST, each lasting 5 minutes, the membranes were treated with horseradish peroxidase-conjugated anti-IgG for 2 hours. The dot blot results were visualized using the Azure 600 Gel Imaging System (Azure Biosystems, Dublin, CA, USA) and quantified with ImageJ software. Methylene blue staining served as the loading control.

RNA decay assay

In brief, actinomycin D (Selleck, Houston, TX, USA) was added to the culture medium at a final concentration of 5 μg/mL. Cells were harvested at 0, 2, and 4 hours. Total RNA was then isolated, and qPCR was conducted to quantify the relative levels of *DYRK1A* mRNA compared to the 0-hour time point.

RNA sequencing

Total RNA was extracted as described above and assessed with an Agilent Bioanalyzer and NanoDrop. High-quality RNA was used for library construction. RNA-seq libraries were prepared using the Illumina Stranded mRNA Prep Ligation kit (Illumina) and sequenced on an Illumina NovaSeq X Plus platform (Cosmos Wisdom, Hangzhou, China).

Colony formation assay

Cells were seeded into 6-well plates (50,000 cells per well) and cultured in the presence of a senescence inducer, as above described. Afterwards, the cells were transfected and cultured for another 2-4 days. At the end of the assay, the cells were fixed with 4% paraformaldehyde for 15 minutes and stained with 0.2% crystal violet staining solution (Beyotime, Shanghai, China) for 15 minutes at room temperature (RT).

Immunofluorescence staining

For the cell immunofluorescence assay, cells were cultured on coverslips and fixed for 15 minutes at room temperature (RT) in 4% paraformaldehyde solution. After fixation, the cells were permeabilized with PBS containing 0.1% Triton X-100 for 10 minutes at RT. The coverslips were then washed with PBS and blocked with 3% bovine serum albumin (BSA) in PBS. The primary antibodies were incubated for 2 hours at RT, followed by incubation with the secondary antibody for 1 hour at RT. Immunofluorescence analysis was performed using the γ-H2AX primary antibody (1:100, ABclonal Technology, USA), DYRK1A (1:100, Bioss, China), and Alexa 568-conjugated anti-rabbit secondary antibody (1:200, Invitrogen, USA).

For the tissue immunofluorescence assay, paraffin-embedded colon tissues were deparaffinized, rehydrated, and subjected to antigen retrieval. The sections were then blocked with 3% bovine serum albumin (BSA) and incubated with the following primary antibodies: anti-Muc2 (Proteintech, 27675-1-AP, 1:500), anti-Ki67 (Servicebio, GB111402, 1:500), anti-Occludin (Servicebio, GB111401, 1:500). After primary antibody incubation, the sections were incubated

with the appropriate secondary antibodies.

Tissue HE staining and IHC analysis

Colon tissues were fixed in 4% paraformaldehyde. Hematoxylin and Eosin (HE) staining and Periodic Acid Schiff (PAS) staining were performed to evaluate morphological changes.

For IHC analysis, we collected formalin-fixed, paraffin-embedded biopsy specimens from 22 healthy donors and 37 patients diagnosed with ulcerative colitis at the Second Affiliated Hospital of Zhejiang University School of Medicine. After deparaffinization, rehydration, antigen retrieval, and blocking of non-specific binding, the sections were incubated overnight at 4°C with NAT10 antibody (Abcam, 1:200) or DYRK1A antibody (Bioss, 1:200). The next day, the sections were treated with secondary antibodies for 50 minutes at room temperature. Following this, the sections were stained with DAB, counterstained with hematoxylin, and observed under a Nikon microscope. The proportion of positive cells was quantified and categorized into four groups: 0 (0–5%), 1 (6%–50%), 2 (51%–75%), and 3 (76%–100%). Staining intensity was graded as follows: 0 for no staining, 1 for weak, 2 for moderate, and 3 for strong staining. The final staining score was obtained by multiplying the positive cell percentage by the staining intensity. Information of human samples is provided in the **Supplementary Table 4.**

DSS-induced colitis model

Acute colitis was induced using DSS (160 110, MP Biomedicals). Two weeks prior to induction, the mice were randomly assigned to different cages for co-housing. They were then administered

a 7-day treatment with 3% DSS via oral gavage. All the mice used in this study were housed in the specific pathogen-free facility of the Laboratory. Experimental procedures were conducted in accordance with the guidelines of the Institutional Animal Use.

For colonoscopy in mice, the animals were fasted for 24 hours and anesthetized with isoflurane. An ENDOQ small animal endoscope (ENDOQ-E1, Siboyu Biotechnology Corporation) was used to perform the colonoscopy.

Nat10$^{+/-}$ mice and mice experiments

Nat10-knockout mice were generated and obtained from Shanghai Model Organisms Center, Inc. Briefly, the Nat10$^{+/-}$ mice used in this study were created by deleting exon 4 using a CRISPR/Cas9-based genome editing approach. Genotyping was performed by PCR with primers flanking the deleted region.

All animal studies were conducted in accordance with the guidelines approved by the Institutional Animal Care and Use Committee of Zhejiang University. All mice used in this study were on a C57BL/6 genetic background and maintained at a specific pathogen-free (SPF) level animal facility in Animal Experiment Center, Zhejiang Chinese Medical University. The ambient temperature was maintained at 20–22°C with a relative humidity of 45–65%. Mice were provided a standard laboratory diet, water and were kept in ventilated cages under a 12-hour light/12-hour dark cycle.

NAT10 and DYRK1A inhibitor treatment

Remodelin was prepared in PEG300 and TW-20 and administered intraperitoneally at a dose of 20 mg/kg. Harmine was prepared in PEG300 and TW-20 and administered intraperitoneally at a dose of 10 mg/kg. A solvent with the same composition and volume was used as the vehicle group.

For mouse enema treatment, the mice were fasted for 24 hours and anesthetized with isoflurane. A polyethylene catheter was inserted into the colon, approximately 4 cm from the anus, and Harmine or vehicle was slowly administered using a syringe. Following the injection, the mice were kept in an inverted vertical position for at least 1 minute. After recovery, the mice were allowed to resume normal water and food intake.

Nat10 knockdown and Dyrk1a expression in mice

All adeno-associated viruses serotype 8 (AAV8) were purchased from Genechem (Shanghai, China). AAV8-shNat10 and AAV8-shNC (CV762 vector with villin promoter) were used to knock down Nat10 expression *in vivo*. The shRNA targeting sequence for mouse Nat10 was 5′-GAGCATCTGGATTATGAGATT-3′. Each mouse received 5.0E+11 v.g of virus via tail-vein injection. Dyrk1a overexpression was achieved using adeno-associated viruses (AAV8-Dyrk1a and AAV8-Vector, The GV411 vector with CMV promoter). Each mouse received 1.0E+12 v.g of virus via tail-vein injection.

Colonoid construction and culture

Colon tissues from C57BL/6 mice were dissected longitudinally and rinsed three times with cold Dulbecco's Phosphate-Buffered Saline (DPBS) containing penicillin–streptomycin to clear out

contents and mucus. The tissues were then cut into small pieces and incubated in 5 mM EDTA on a rotor at 4°C for 40 minutes. Crypts were released by mechanical shearing with pipette tips in PBS with 0.01% BSA. After passing through a 100 μm cell strainer, 200 crypts were combined with 50 μl of Matrigel (Corning #356231) and plated as a dome in the center of a pre-warmed 24-well plate. The plate was incubated at 37°C with 5% CO2 for 10 minutes to solidify. Complete Intesticult medium (Stemcell Technologies #06005) was added to support colonoid growth and replaced every 3 days. Passaging was performed after 7 days of culture.

For the in vitro lipopolysaccharide (LPS) treatment experiment, LPS (Sigma-Aldrich, L4391, USA) was added to the complete culture medium at a concentration of 5 μg/ml for colonoid cultivation. On day 3 of the culture period, the medium was replaced with LPS-containing medium. For the NAT10 inhibitor experiment, the NAT10 inhibitor Re (10 μM) or vehicle was added to the complete colonoid medium. Colonoids were photographed daily starting from day 7 of the culture period using an inverted microscope to evaluate regenerative growth.

Statistics and reproducibility

Each experiment was performed with at least three biological replicates. Representative images for fluorescence staining, PAS staining, H&E staining and SA-Gal staining are shown, each of these experiments included at least three independent samples and was repeated at least three times. Statistical analyses were performed using GraphPad Prism 10.0 Software (GraphPad, Inc., San Diego, CA, USA). Data were expressed as mean ± SD (standard deviation). Differences between groups were analyzed by Two-tailed unpaired Student's t-test and two-way ANOVA with Tukey's

multiple comparisons. Correlations were performed using the Spearman correlation test. A p-value <0.05 was regarded as statistically significant. No statistical method was used to predetermine the sample size. The sample sizes ("n") and the statistical tests are described in each figure legend, exact p values are provided in the Source Data (*p < 0.05, **p <0.01, and ***p <0.001).

Reporting summary

Further information on research design is available in the Nature Portfolio Reporting Summary linked to this article.

Data availability

The RNA-seq data generated in this study have been deposited in the SRA database under accession code PRJNA1394239 (https://www.ncbi.nlm.nih.gov/sra/?term=PRJNA1394239). The acRIP-seq data generated in this study have been deposited in the SRA database under accession code PRJNA1347399 (https://www.ncbi.nlm.nih.gov/sra/?term=PRJNA1347399). Other data from the findings of this study are available from the corresponding author upon request. Source data are provided with this paper.

References

1. Kennedy, B.K. *et al.* Geroscience: linking aging to chronic disease. *Cell* **159**, 709-713 (2014).
2. Campisi, J. *et al.* From discoveries in ageing research to therapeutics for healthy ageing.

Nature **571**, 183-192 (2019).

3. Hohman, L.S. & Osborne, L.C. A gut-centric view of aging: Do intestinal epithelial cells contribute to age-associated microbiota changes, inflammaging, and immunosenescence? *Aging Cell* **21**, e13700 (2022).
4. Cai, Y. *et al.* The landscape of aging. *Sci China Life Sci* (2022).
5. Wang, Q. *et al.* The Aged Intestine: Performance and Rejuvenation. *Aging Dis* **12**, 1693-1712 (2021).
6. Liu, A. *et al.* Aging Increases the Severity of Colitis and the Related Changes to the Gut Barrier and Gut Microbiota in Humans and Mice. *J Gerontol A Biol Sci Med Sci* **75**, 1284-1292 (2020).
7. Sun, T.Y. *et al.* MiR-1-3p and MiR-124-3p Synergistically Damage the Intestinal Barrier in the Ageing Colon. *J Crohns Colitis* **16**, 656-667 (2022).
8. Hu, X. *et al.* Intestinal Epithelial Cell-specific Deletion of Cytokine-inducible SH2-containing Protein Alleviates Experimental Colitis in Ageing Mice. *J Crohns Colitis* **17**, 1278-1290 (2023).
9. Huang, L. *et al.* Elevated miR-124-3p in the aging colon disrupts mucus barrier and increases susceptibility to colitis by targeting T-synthase. *Aging Cell* **19**, e13252 (2020).
10. Sienkiewicz, M., Sroka, K., Binienda, A., Jurk, D. & Fichna, J. A new face of old cells: An overview about the role of senescence and telomeres in inflammatory bowel diseases. *Ageing Res Rev* **91**, 102083 (2023).
11. Ruel, J., Ruane, D., Mehandru, S., Gower-Rousseau, C. & Colombel, J.F. IBD across the age spectrum: is it the same disease? *Nat Rev Gastroenterol Hepatol* **11**, 88-98 (2014).
12. Agrawal, M. *et al.* The Rising Burden of Inflammatory Bowel Disease in Denmark Over Two Decades: A Nationwide Cohort Study. *Gastroenterology* **163**, 1547-1554 e1545 (2022).
13. Ha, C.Y. & Katz, S. Clinical implications of ageing for the management of IBD. *Nat Rev Gastroenterol Hepatol* **11**, 128-138 (2014).

14. Sousa, P., Bertani, L. & Rodrigues, C. Management of inflammatory bowel disease in the elderly: A review. *Dig Liver Dis* **55**, 1001-1009 (2023).
15. Rozich, J.J., Dulai, P.S., Fumery, M., Sandborn, W.J. & Singh, S. Progression of Elderly Onset Inflammatory Bowel Diseases: A Systematic Review and Meta-Analysis of Population-Based Cohort Studies. *Clin Gastroenterol Hepatol* **18**, 2437-2447 e2436 (2020).
16. Bollegala, N., Jackson, T.D. & Nguyen, G.C. Increased Postoperative Mortality and Complications Among Elderly Patients With Inflammatory Bowel Diseases: An Analysis of the National Surgical Quality Improvement Program Cohort. *Clin Gastroenterol Hepatol* **14**, 1274-1281 (2016).
17. Meng, G., Monaghan, T.M., Duggal, N.A., Tighe, P. & Peerani, F. Microbial-Immune Crosstalk in Elderly-Onset Inflammatory Bowel Disease: Unchartered Territory. *J Crohns Colitis* (2023).
18. Clevers, H. & Batlle, E. SnapShot: the intestinal crypt. *Cell* **152**, 1198-1198 e1192 (2013).
19. Di Micco, R., Krizhanovsky, V., Baker, D. & d'Adda di Fagagna, F. 1-Cellular senescence in ageing: from mechanisms to therapeutic opportunities. *Nat Rev Mol Cell Biol* **22**, 75-95 (2021).
20. Lopez-Otin, C., Blasco, M.A., Partridge, L., Serrano, M. & Kroemer, G. Hallmarks of aging: An expanding universe. *Cell* **186**, 243-278 (2023).
21. Wang, K. *et al.* Epigenetic regulation of aging: implications for interventions of aging and diseases. *Signal Transduct Target Ther* **7**, 374 (2022).
22. Sun, H., Li, K., Liu, C. & Yi, C. Regulation and functions of non-m(6)A mRNA modifications. *Nat Rev Mol Cell Biol* **24**, 714-731 (2023).
23. Arango, D. *et al.* Acetylation of Cytidine in mRNA Promotes Translation Efficiency. *Cell* **175**, 1872-1886 e1824 (2018).
24. Dalhat, M.H., Narayan, S., Serio, H. & Arango, D. Dissecting the oncogenic properties of essential RNA-modifying enzymes: a focus on NAT10. *Oncogene* **43**, 1077-1086 (2024).
25. Liu, R. *et al.* NAT10-mediated N4-acetylcytidine mRNA modification regulates self-

renewal in human embryonic stem cells. *Nucleic Acids Res* **51**, 8514-8531 (2023).

26. Chen, L. *et al.* NAT10-mediated N4-acetylcytidine modification is required for meiosis entry and progression in male germ cells. *Nucleic Acids Res* **50**, 10896-10913 (2022).
27. Huang, W., Hickson, L.J., Eirin, A., Kirkland, J.L. & Lerman, L.O. Cellular senescence: the good, the bad and the unknown. *Nat Rev Nephrol* **18**, 611-627 (2022).
28. Liu, H. *et al.* Targeting N4-acetylcytidine suppresses hepatocellular carcinoma progression by repressing eEF2-mediated HMGB2 mRNA translation. *Cancer Commun (Lond)* (2024).
29. Hunt, D.P.J. & Hofer, M.J. Unweaving type I interferons in age-related neuroinflammation. *Trends Neurosci* **47**, 751-752 (2024).
30. Chen, X. *et al.* The role of oxidative stress in intervertebral disc degeneration: Mechanisms and therapeutic implications. *Ageing Res Rev* **98**, 102323 (2024).
31. Liu, D. *et al.* NAT10 promotes synovial aggression by increasing the stability and translation of N4-acetylated PTX3 mRNA in rheumatoid arthritis. *Ann Rheum Dis* **83**, 1118-1131 (2024).
32. Qi, Y. *et al.* Heat-inactivated Bifidobacterium adolescentis ameliorates colon senescence through Paneth-like-cell-mediated stem cell activation. *Nat Commun* **14**, 6121 (2023).
33. He, D. *et al.* Gut stem cell aging is driven by mTORC1 via a p38 MAPK-p53 pathway. *Nat Commun* **11**, 37 (2020).
34. Omrani, O. *et al.* IFNgamma-Stat1 axis drives aging-associated loss of intestinal tissue homeostasis and regeneration. *Nat Commun* **14**, 6109 (2023).
35. Wang, Z. *et al.* FUT2-dependent fucosylation of HYOU1 protects intestinal stem cells against inflammatory injury by regulating unfolded protein response. *Redox Biol* **60**, 102618 (2023).
36. Zheng, X. *et al.* N-acetyltransferase 10 promotes colon cancer progression by inhibiting ferroptosis through N4-acetylation and stabilization of ferroptosis suppressor protein 1 (FSP1) mRNA. *Cancer Commun (Lond)* **42**, 1347-1366 (2022).
37. Yang, W. *et al.* ac4C acetylation of RUNX2 catalyzed by NAT10 spurs osteogenesis of

BMSCs and prevents ovariectomy-induced bone loss. *Mol Ther Nucleic Acids* **26**, 135-147 (2021).

38. Xie, R. *et al.* NAT10 Drives Cisplatin Chemoresistance by Enhancing ac4C-Associated DNA Repair in Bladder Cancer. *Cancer Res* **83**, 1666-1683 (2023).
39. Guo, G. *et al.* Epitranscriptomic N4-Acetylcytidine Profiling in CD4(+) T Cells of Systemic Lupus Erythematosus. *Front Cell Dev Biol* **8**, 842 (2020).
40. Balmus, G. *et al.* Targeting of NAT10 enhances healthspan in a mouse model of human accelerated aging syndrome. *Nat Commun* **9**, 1700 (2018).
41. Rammohan, M. *et al.* The chromosome 21 kinase DYRK1A: emerging roles in cancer biology and potential as a therapeutic target. *Oncogene* **41**, 2003-2011 (2022).
42. Litovchick, L., Florens, L.A., Swanson, S.K., Washburn, M.P. & DeCaprio, J.A. DYRK1A protein kinase promotes quiescence and senescence through DREAM complex assembly. *Genes Dev* **25**, 801-813 (2011).
43. Park, J. *et al.* Dyrk1A phosphorylates p53 and inhibits proliferation of embryonic neuronal cells. *J Biol Chem* **285**, 31895-31906 (2010).
44. Chen, J.Y., Lin, J.R., Tsai, F.C. & Meyer, T. Dosage of Dyrk1a shifts cells within a p21-cyclin D1 signaling map to control the decision to enter the cell cycle. *Mol Cell* **52**, 87-100 (2013).
45. Soppa, U. *et al.* The Down syndrome-related protein kinase DYRK1A phosphorylates p27(Kip1) and Cyclin D1 and induces cell cycle exit and neuronal differentiation. *Cell Cycle* **13**, 2084-2100 (2014).
46. Hu, K. *et al.* MicroRNA-221-3p inhibits the inflammatory response of keratinocytes by regulating the DYRK1A/STAT3 signaling pathway to promote wound healing in diabetes. *Commun Biol* **7**, 300 (2024).
47. Bhansali, R.S. *et al.* DYRK1A regulates B cell acute lymphoblastic leukemia through phosphorylation of FOXO1 and STAT3. *J Clin Invest* **131** (2021).
48. Murray, A. *et al.* Dose imbalance of DYRK1A kinase causes systemic progeroid status in

Down syndrome by increasing the un-repaired DNA damage and reducing LaminB1 levels. *EBioMedicine* **94**, 104692 (2023).

49. Kim, M.Y. *et al.* A repressor complex, AP4 transcription factor and geminin, negatively regulates expression of target genes in nonneuronal cells. *Proc Natl Acad Sci U S A* **103**, 13074-13079 (2006).
50. Wang, P., Wang, L., Chen, L. & Sun, X. Dual-specificity tyrosine-phosphorylation regulated kinase 1A Gene Transcription is regulated by Myocyte Enhancer Factor 2D. *Sci Rep* **7**, 7240 (2017).
51. Saccon, T.D. *et al.* Senolytic Combination of Dasatinib and Quercetin Alleviates Intestinal Senescence and Inflammation and Modulates the Gut Microbiome in Aged Mice. *J Gerontol A Biol Sci Med Sci* **76**, 1895-1905 (2021).
52. Zhou, M., Liu, Z.L., Liu, J.Y. & Wang, X.B. Tedizolid phosphate alleviates DSS-induced ulcerative colitis by inhibiting senescence of cell and colon tissue through activating AMPK signaling pathway. *Int Immunopharmacol* **135**, 112286 (2024).
53. Wellman, A.S. *et al.* Intestinal Epithelial Sirtuin 1 Regulates Intestinal Inflammation During Aging in Mice by Altering the Intestinal Microbiota. *Gastroenterology* **153**, 772-786 (2017).
54. Zhao, Y., Simon, M., Seluanov, A. & Gorbunova, V. DNA damage and repair in age-related inflammation. *Nat Rev Immunol* **23**, 75-89 (2023).
55. Bao, W. *et al.* Inhibiting sorting nexin 10 promotes mucosal healing through SREBP2-mediated stemness restoration of intestinal stem cells. *Sci Adv* **9**, eadh5016 (2023).
56. Gonzalez, E.A. *et al.* TET3-mediated DNA oxidation is essential for intestinal epithelial cell response to stressors. *Proc Natl Acad Sci U S A* **120**, e2221405120 (2023).
57. Ren, X. *et al.* DHX9 maintains epithelial homeostasis by restraining R-loop-mediated genomic instability in intestinal stem cells. *Nat Commun* **15**, 3080 (2024).
58. Choi, Y.W. *et al.* Senescent Tumor Cells Build a Cytokine Shield in Colorectal Cancer. *Adv Sci (Weinh)* **8**, 2002497 (2021).

59. Tollefsbol, T.O. Biological Aging: Methods and Protocols. *Methods in Molecular Biology* **1048** (2013).

Acknowledgments

We thank Xiaoyu Li (Zhejiang University School of Medicine) and Liang Lu (Zhejiang University) for their helpful discussions and technical support in the detection and analysis of RNA modifications. We thank Chunchun Li, Xiaoye Li, Liya Lin and Jiaying Li (Clinical Research Center, The Second Affiliated Hospital of Zhejiang University School of Medicine) for the laboratory management and technical support. We thank Yunlu Chen, Hui Xie and Zhenlin Jiang (Animal Experiment Center, The Second Affiliated Hospital of Zhejiang University School of Medicine) for their technical support in small animal endoscopy techniques. This project was financially supported by National Foundation of Natural Science of China (82525010 to S.C.) and Provincial Key R&D Program of Zhejiang (2023C03163 to L.W.).

Author Contributions Statement

S.C., L.W. and M.X. designed and supervised the study. J.C. performed most experiments with the assistance of S.M., A.F., W.C., Y.S., S.X., Q.G., J.L. and Q.Y.; J.C. and M.X. analyzed and interpreted the data. J.C. drafted the manuscript. S.C. and L.W. critically revised the manuscript.

Competing Interests Statement

The authors declare no competing interests.

Figure Legends

Figure.1 NAT10 and mRNA ac^{4}C modification are upregulated in the senescent colon epithelial cells.

a, Flow diagram of mRNA modification screening. m/z, mass-to-charge ratio. Created in BioRender. Chen, J. (2026) https://BioRender.com/h61m193. **b**, Analysis of SA-Gal activity in proliferation, H-Sen and D-Sen cells of NCM460 and CCD841. The SA-Gal-positive percentages in senescent cell groups were compared to proliferation cells group. H-Sen, D-Sen: senescent cell induced by H_2O_2 or DOX. Scale bar for NCM460, 100μm. Scale bar for CCD841, 50μm. n=3

independent experiments. Data were represented as mean ± SD. **c-d**, mRNA modification levels in proliferation cells and senescent cell groups of NCM460 and CCD841. n=3 independent experiments. Data were represented as mean ± SD and represented relative to control. **e**, Dot blot of RNA ac^4C modification level and western blot of Cyclin D1, γ-H2AX, p53, p21, p16 and NAT10 in senescent NCM460 and CCD841 cells. **f**, Cell morphology and SA-Gal staining of P5 and P20 CCD841 cells. Scale bar, 50μm. n=3 independent experiments. Data were represented as mean ± SD. **g**, mRNA ac^4C modification level in P5 and P20 CCD841cells. n=3 independent experiments. Data were represented as mean ± SD. Comparisons were performed by Two-tailed unpaired Student's t-test (**b, c, d, f, g**). *** $p<0.001$, ** $p<0.01$, ns $p>0.05$. Source data and exact p value are provided as a Source data file.

Figure.2 NAT10 regulates colon epithelial cell senescence phenotypes through mRNA ac^4C modification

a, Dot blot of RNA ac^4C modification levels in NAT10-reexpressed (NAT10-WT or NAT10-MUT) NCM460 cells after transfected with NAT10-Si and treated with H_2O_2 or DOX. n=3 independent experiments. Data were represented as mean ± SD. **b**, Western blot of NAT10, CyclinD1, γ-H2AX, p21, p53, and p16 in NAT10-reexpressed (NAT10-WT or NAT10-MUT) cells after transfected with NAT10-Si and treated with H_2O_2 or DOX. **c**, Analysis of SA-Gal activity and positive immunofluorescence staining of γ-H2AX in NAT10-reexpressed NCM460 cells after transfected with NAT10 siRNA and treated with H_2O_2. Scale bar for SA-Gal, 100μm. Scale bar for IF, 20μm. n=3 independent experiments. Data were represented as mean ± SD. **d**, Flow diagram for senescent

cell viability and caspase3/7 activity detection. Created in BioRender. Chen, J. (2026) https://BioRender.com/w97m115. **e**, Colony formation assay using H-Sen NCM460 cells after co-transfection of NAT10-Si with either NAT10-WT or NAT10-MUT. **f**, Cell viability analysis in H-Sen NCM460 cells after co-transfection of NAT10-Si with either NAT10-WT or NAT10-MUT. n=3 independent experiments. Data were represented as mean ± SD. **g**, Caspase3/7 activity analysis in H-Sen NCM460 cells after co-transfection of NAT10-Si with either NAT10-WT or NAT10-MUT. n=3 independent experiments. Data were represented as mean ± SD. **h**, Apoptosis flow cytometry analysis in H-Sen NCM460 cells after co-transfection of NAT10-Si with either NAT10-WT or NAT10-MUT. n=3 independent experiments. Data were represented as mean ± SD. Comparisons were performed by Two-tailed unpaired Student's t-test (**a, c, f, g, h**). *** $p<0.001$, ** $p<0.01$, ns $p>0.05$. Source data and exact p value are provided as a Source data file.

Figure.3 Nat10 downregulation preserves epithelial renewal and reduces senescence in the aged colon

a, Immunofluorescence analysis of Nat10 expression in 2-mon, 6-mon,12-mon, and 18-mon mice colon. Scale bar, 100 μm. **b**, Western blot analysis of Nat10 in the colon of 2-mon, 6-mon,12-mon, and 18-mon mice. mon, month. **c**, The schematic diagram of the WT and $Nat10^{+/-}$ mice experimental procedure. Created in BioRender. Chen, J. (2026) https://BioRender.com/x16w213. **d**, Western blot analysis of Nat10, Ocln, Lgr5, p53 p21, and p16 in colon tissues from Young-WT, Aged-WT (12-mon), and Aged-$Nat10^{+/-}$ (12-mon) mice. **e**, Hematoxylin-eosin staining and immunofluorescence staining of Nat10, Ocln, Ki67, and Muc2 in colon tissues from Young-WT,

Aged-WT, and Aged-Nat10$^{+/-}$ mice groups. The mucosal height was measured. n=15 random fields per group. The mean fluorescence intensity of 10 fields was normalized to the Young-WT group. Ki67^{+} and Muc2^{+} cells were quantified from 30 fields for comparison. The median positive cell number per crypt from each field was used for comparison. Scale bar, 50 μm. Data were represented as mean ± SD. **f**, Western blot analysis of Nat10, p21, and p16 in colon tissues from aged WT mice (18 months) after two months tail-vein injection of AAV-NC or AAV-shNat10. **g,** Hematoxylin–eosin staining and immunofluorescence for Ocln and Ki67 in colon tissues from the same aged WT mice, two months after tail-vein injection of AAV-NC or AAV-shNat10. Scale bar, 100 μm. AAV, adeno-associated virus. Data are presented as mean values ± S.D. Comparisons were performed by Two-tailed unpaired Student's t-test (**e**). *** p<0.001, ** p<0.01**.** Source data and exact p value are provided as a Source data file.

Figure.4 DYRK1A as a target of mRNA ac^{4}C modification in regulating colon epithelial cell senescence

a, Schematic illustration of acRIP-seq in NCM460 cells. Created in BioRender. Chen, J. (2026) https://BioRender.com/j92d013. **b**, Pie charts showed the distribution of ac^{4}C peak in the acetylated transcripts in the control NC-Si, H-Sen NC-Si, and H-Sen NAT10-Si groups. **c**, GO-BP enrichment analysis of hyperacetylated genes in H-Sen NCM460 cells compared to control NCM460 cells (left). GO-BP enrichment analysis of hypoacetylated genes in H-Sen NCM460 cells with NAT10-Si compared to H-Sen NCM460 cells with NC-Si (right). **d**, Overlapping the potential downstream targets of NAT10-meditated RNA ac^{4}C modification in hyperacetylated gene (H-Sen NC-Si vs Control NC-Si) and hypoacetylated gene (H-Sen NAT10-Si vs H-Sen NC-Si) by the

acRIP-seq analysis. **e**, acRIP-qPCR validation of ac^4C level alterations in four potential downstream targets across the control NC-Si, H-Sen NC-Si, and H-Sen NAT10-Si groups. n=3 independent experiments. Data were represented as mean ± SD. **f**, qPCR was used to validate *DYRK1A* and *LMLN* RNA expression across the three groups. n=3 independent experiments. Data were represented as mean ± SD. **g,** Actinomycin D (ActD) chase RNA-seq showing DYRK1A mRNA level change in H-Sen NC-Si and H-Sen NAT10-Si cells. n=3 independent samples. Data were represented as mean ± SD. **h,** IGV plots showed that ac^4C peaks changes in the CDS domains of DYRK1A mRNA in the control NC-Si, H-Sen NC-Si, and H-Sen NAT10-Si groups from acRIP-seq data. **i,** RNA ac^4C modifications and THAP5, DYRK1A and LMLN protein levels were detected by dot blot or western blot across the three groups. Two-way ANOVA analysis with Tukey's multiple comparison was used for (**g**). Two-tailed unpaired Student's t-test was used for other analyses (**e, f**). *** $p<0.001$, ** $p<0.01$, ns $p>0.05$. Source data and exact p value are provided as a Source data file.

Figure.5 NAT10 promotes colon epithelial cell senescence by ac4C-mediated regulation of *DYRK1A* mRNA.

a, acRIP-qPCR analysis of ac^4C levels in CDS domain of *DYRK1A* among control, H-Sen, and D-Sen NCM460 cells. n=3 independent experiments. Data were represented as mean ± SD. **b**, DYRK1A mRNA expression and protein expression in control, H-Sen, and D-Sen NCM460 cells. n=3 independent experiments. Data were represented as mean ± SD. **c**, Immunofluorescence staining of DAPI, γ-H2AX, and DYRK1A in control, H-Sen, and D-Sen NCM460 cells. Scale bar

for immunofluorescence, 20 μm. **d**, Immunoblotting of NAT10 after NAT10-RIP assay with cell lysate among control, H-Sen, and D-Sen NCM460 cells. qPCR analysis of CDS domain of *DYRK1A* was performed after NAT10-RIP. n=3 independent experiments. Data were represented as mean ± SD. **e**, *DYRK1A* mRNA stability was measured by adding actinomycin D in control, H-Sen, D-Sen NCM460 cells and in H-Sen and D-Sen NCM460 cells with NAT10 knockdown. n=3 independent experiments. Data were represented as mean ± SD. **f.** Sucrose gradient fractionation of H-Sen NCM460 cells and H-Sen NCM460 cells with NAT10 knockdown. Relative *DYRK1A* mRNA abundance across polysome fraction was quantified by RT-qPCR. n=3 independent experiments. Data were represented as mean ± SD. **g**, Analysis of SA-Gal activity in DYRK1A-reexpressed NCM460 cells after transfected with NAT10 siRNA and treated with H_2O_2 or DOX. Scale bar for SA-Gal, 100 μm. **h**, qPCR analysis of *IL-1β* and *IL-6* in DYRK1A-reexpressed NCM460 cells after transfected with NAT10 siRNA and treated with H_2O_2 or DOX. n=3 independent experiments. Data were represented as mean ± SD. **i**, Western blot of NAT10, DYRK1A, γ-H2AX, and p21 in DYRK1A-reexpressed cells after transfected with NAT10-Si and treated with H_2O_2 or DOX. **j**, Caspase3/7 activity analysis in DYRK1A-reexpressed H-Sen and D-Sen NCM460 cells after transfected with NAT10-Si. n=3 independent experiments. Data were represented as mean ± SD. Two-way ANOVA analysis with Tukey's multiple comparison was used for (**e**). Two-tailed unpaired Student's t-test was used for other analyses (**a, b, d, e, f, g, h, j**). *** $p<0.001$, ** $p<0.01$, * $p<0.05$. Source data and exact p value are provided as a Source data file.

Figure.6 Deficiency of Nat10 Enhances Colonoid Performance and Mitigates LPS-Induced Proliferation Loss in Aged Mice

a, The schematic diagram of colonoid extraction from aged mice. Created in BioRender. Chen, J. (2026) https://BioRender.com/n10d667. **b**, Representative brightfield images and EdU immunofluorescence of Young-WT, Aged-WT, and Aged-Nat10$^{+/-}$ colonoids after 7 days of culture. Scale bar for brightfield, 200 μm. Scale bar for immunofluorescence, 50 μm. n=3 independent experiments. Data were represented as mean ± SD. **c**, Comparative analysis of the growth status of budding colonoid at different time points (3 days, 5 days, and 7 days). Relative colonoid size of 5 days and 7 days were normalized to the 3 days. n=3 independent experiments. Data were represented as mean ± SD. **d**, Western blot of Lgr5, and Nat10 in Young-WT, Aged-WT, and Aged-Nat10$^{+/-}$ colonoids. **e-f**, *p21, pcna* **(e)** *and Muc2* **(f)** mRNA level in Young-WT, Aged-WT, and Aged-Nat10$^{+/-}$ colonoids. n=3 independent experiments. Data were represented as mean ± SD. **g**, The schematic diagram of in vitro colonoid LPS treatment. Created in BioRender. Chen, J. (2026) https://BioRender.com/k88n403. **h**, qPCR analysis of *Lgr5* expression in Aged-WT, Aged-Nat10$^{+/-}$, and qPCR analysis of *Lgr5* in Aged-WT+Vehicle, Aged-WT+Rem after LPS treatment. n=3 independent experiments. Data were represented as mean ± SD. **i-j**, Representative brightfield images of colonoids (day7) in Aged-WT, Aged-Nat10$^{+/-}$, Aged-WT+Vehicle and Aged-WT+Rem colonoids after LPS treatment. Scale bar, 100 μm. The percentage of budding colonoids was compared. n=3 independent experiments. Data were represented as mean ± SD. **K**, Western blot of Dyrk1a and γ-H2AX in Aged-WT, Aged-Nat10$^{+/-}$, and in Aged-WT+Vehicle, Aged-WT+Rem after LPS treatment. Two-way ANOVA analysis with Tukey's multiple comparison was used for

(**c**). Two-tailed unpaired Student's t-test was used for other analyses **(b, e, f, h, j)**. *** $p<0.001$, ** $p<0.01$, * $p<0.05$. Source data and exact p value are provided as a Source data file.

Figure.7 Deficiency of Nat10 in aged mice alleviates DSS-induced colitis

a, Schematic diagram showing that the process of DSS-induced acute colitis in aged (12-mon) Nat10-WT and $Nat10^{+/-}$ mice. Created in BioRender. Chen, J. (2026) https://BioRender.com/dn0esiu. **b**, Monitoring of body weight changes throughout the process of DSS-induced acute colitis in aged Nat10-WT and $Nat10^{+/-}$ mice. n=5 animals per group. Data are presented as mean values ± S.D. **c**, Representative image and length analysis of the mouse colon. n=5 animals per group. **d,** Representative colonoscopy images and scores analysis of colon mucosa on day 11. n=5 animals per group. Data are presented as mean values ± S.D. **e,** Pathological score analysis of colonic mucosa. n=5 animals per group. Data are presented as mean values ± S.D. **f,** Dot blot analysis of RNA ac^4C modification levels in the colon. Quantification of relative ac^4C modification intensity was calculated by quantifying the gray value of ac^4C/MB. n=5 animals per group. Data are presented as mean values ± S.D. **g-h**, Immunofluorescence staining of γ-H2AX, Ki67 and PAS staining in colon tissues. $γ\text{-H2AX}^+$ and $Ki67^+$ cells were quantified from 15 random fields per group for comparison, Scale bar, 100 μm. **i**, Relative mRNA levels of *p21, Il-1β, Il-6* and *Tnf-α* in the colon of Aged-WT and Aged-$Nat10^{+/-}$ mice. Data are presented as mean values ± S.D. **j**, Western blot analysis of Nat10, Dyrk1a, Ocln and γ-H2AX in colon tissues from Aged-WT and Aged-$Nat10^{+/-}$ mice following DSS exposure. **l**, Schematic showing the timeline of DSS-induced colitis after 2-month AAV tail-vein delivery. Created in BioRender. Shuyi, M. (2026)

https://BioRender.com/p2dg8is. **m,** Monitoring of body weight changes throughout the process of DSS-induced colitis after 2-month AAV tail-vein delivery. n=5. **n,** Representative HE staining and pathological scores of colonic mucosa from aged mice treated with DSS following 2-month AAV tail-vein delivery (NC+Vector, shNat10+Vector, or shNat10+Dyrk1a). Scale bar, 100 μm. n=5. Data are presented as mean values ± S.D. Body weight changes over time (**b,m**) were analyzed by two-way ANOVA with Tukey's multiple comparison. Two-tailed unpaired Student's t-test was used for other analyses. *** $p<0.001$, ** $p<0.01$, * $p<0.05$**.** Source data and exact p value are provided as a Source data file.

Figure.8 NAT10 and DYRK1A expression are elevated in the aged colon and elderly UC tissues.

a-c, Representative IHC staining image and IHC score of NAT10 and DYRK1A in the colonic mucosa of Young HC (n=10), Old-HC (n=12), Young-UC (n=21) and Old-UC (n=16) patients. Scale bar, 50 μm. **d,** Correlation analysis between NAT10 and DYRK1A immunohistochemical scores in colonic mucosal biopsies from UC patients. **e,** Comparison of NAT10 or DYRK1A immunohistochemical scores among old UC patients stratified by endoscopic Mayo score (Mayo 0-1, Mayo 2-3). n=6 individuals for Mayo0-1 group, n=10 individuals for Mayo2-3 group. The box plots (**b, c, e**) show the median (centre line), the 25th and 75th percentiles (box bounds), and the minimum (lower whiskers) and maximum values (upper whiskers). Spearman correlation analysis was used for (**d**). Two-tailed unpaired Student's t-test was used for other analyses (**b, c, e**). *** $p<0.001$, ** $p<0.01$, * $p<0.05$**.** Source data and exact p value are provided as a Source data

file.

Editorial Summary

This study identifies NAT10-mediated RNA ac4C modification as a key regulator of colonic epithelial aging. Through N4-acetylation regulation of DYRK1A, NAT10 promotes intestinal senescence, highlighting a potential therapeutic target for elderly-onset colitis.

Peer review information: *Nature Communications* thanks the anonymous reviewers for their contribution to the peer review of this work. A peer review file is available.

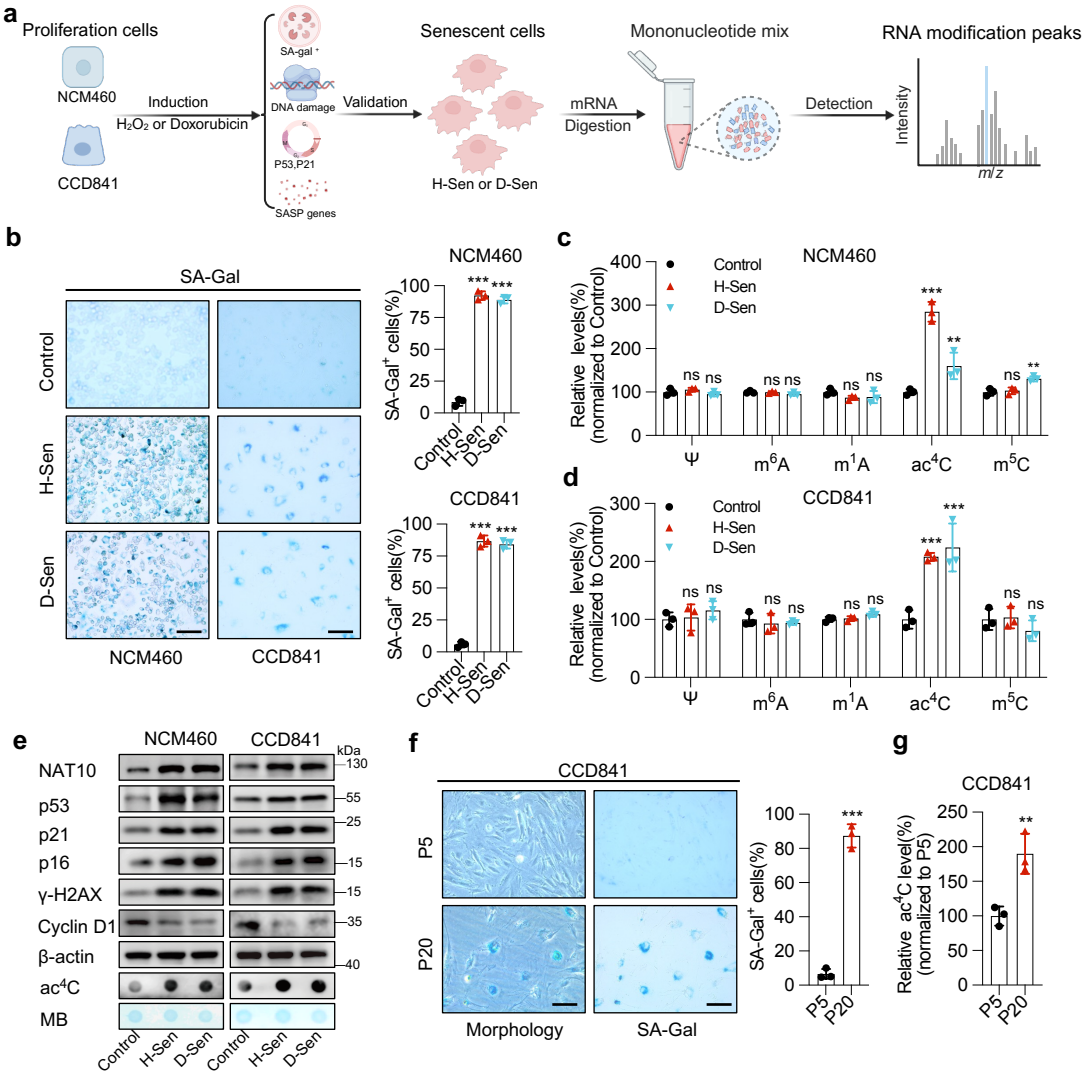
a
Proliferation cells
NCM460
CCD841
Induction
H2O2 or Doxorubicin
SA-gal +
DNA damage
P53,P21
SASP genes
Validation
Senescent cells
H-Sen or D-Sen
mRNA
Digestion
Mononucleotide mix
Detection
RNA modification peaks
Intensity
m/z
b
SA-Gal
Control
H-Sen
D-Sen
NCM460
CCD841
SA-Gal+ cells(%)
c
NCM460
Control
H-Sen
D-Sen
Relative levels(%)
(normalized to Control)
Ψ
m6A
m1A
ac4C
m5C
d
CCD841
e
NCM460
CCD841
kDa
NAT10
p53
p21
p16
γ-H2AX
Cyclin D1
β-actin
ac4C
MB
130
55
25
15
15
35
40
f
CCD841
P5
P20
Morphology
SA-Gal
SA-Gal+ cells(%)
g
CCD841
Relative ac4C level(%)
(normalized to P5)

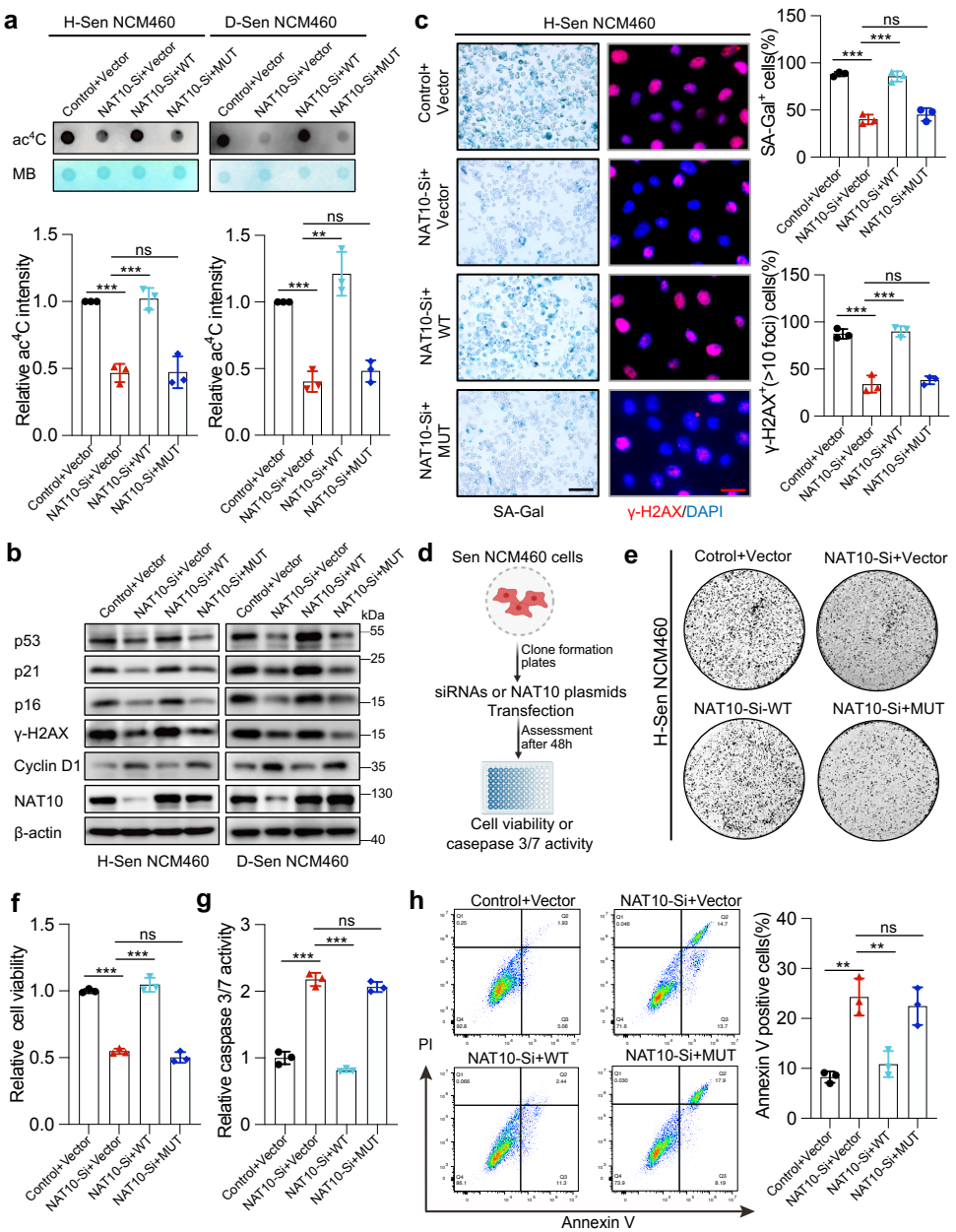
a
H-Sen NCM460
D-Sen NCM460
Control+Vector
NAT10-Si+Vector
NAT10-Si+WT
NAT10-Si+MUT
ac4C
MB
Relative ac4C intensity
b
kDa
p53
p21
p16
γ-H2AX
Cyclin D1
NAT10
β-actin
c
SA-Gal
γ-H2AX/DAPI
SA-Gal+ cells(%)
γ-H2AX+(>10 foci) cells(%)
d
Sen NCM460 cells
Clone formation plates
siRNAs or NAT10 plasmids Transfection
Assessment after 48h
Cell viability or casepase 3/7 activity
e
Cotrol+Vector
NAT10-Si+Vector
NAT10-Si-WT
NAT10-Si+MUT
f
Relative cell viability
g
Relative caspase 3/7 activity
h
PI
Annexin V
Annexin V positive cells(%)

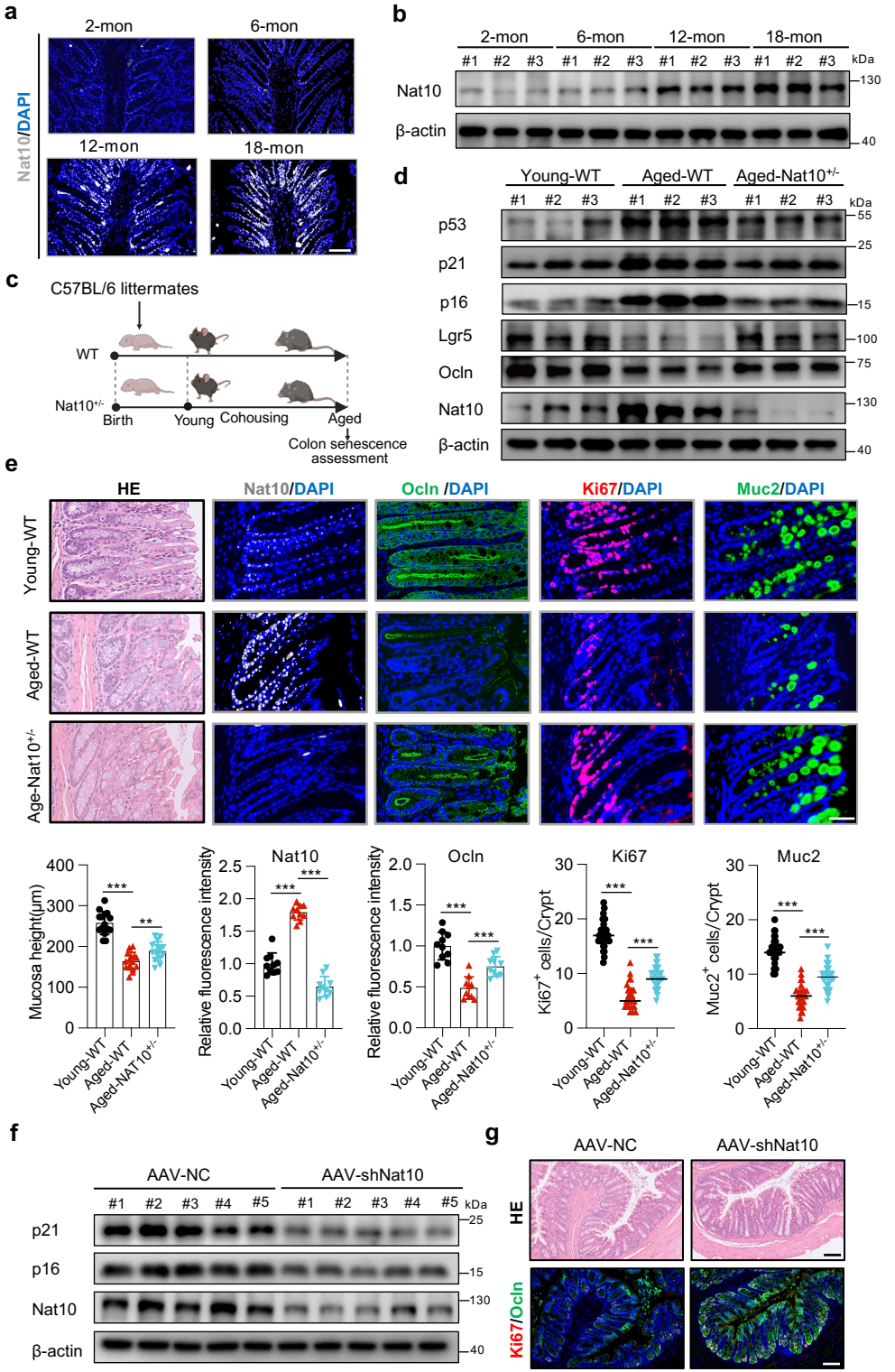
a
2-mon
6-mon
12-mon
18-mon
Nat10/DAPI
b
2-mon
6-mon
12-mon
18-mon
#1 #2 #3 #1 #2 #3 #1 #2 #3 #1 #2 #3
kDa
Nat10
β-actin
130
40
c
C57BL/6 littermates
WT
Nat10+/-
Birth
Young
Cohousing
Aged
Colon senescence assessment
d
Young-WT
Aged-WT
Aged-Nat10+/-
#1 #2 #3 #1 #2 #3 #1 #2 #3
kDa
p53
p21
p16
Lgr5
Ocln
Nat10
β-actin
55
25
15
100
75
130
40
e
HE
Nat10/DAPI
Ocln /DAPI
Ki67/DAPI
Muc2/DAPI
Young-WT
Aged-WT
Age-Nat10+/-
Mucosa height(μm)
Relative fluorescence intensity
Nat10
Ocln
Ki67+ cells/Crypt
Muc2+ cells/Crypt
Young-WT
Aged-WT
Aged-NAT10+/-
Aged-Nat10+/-
f
AAV-NC
AAV-shNat10
#1 #2 #3 #4 #5 #1 #2 #3 #4 #5
kDa
p21
p16
Nat10
β-actin
25
15
130
40
g
AAV-NC
AAV-shNat10
HE
Ki67/Ocln

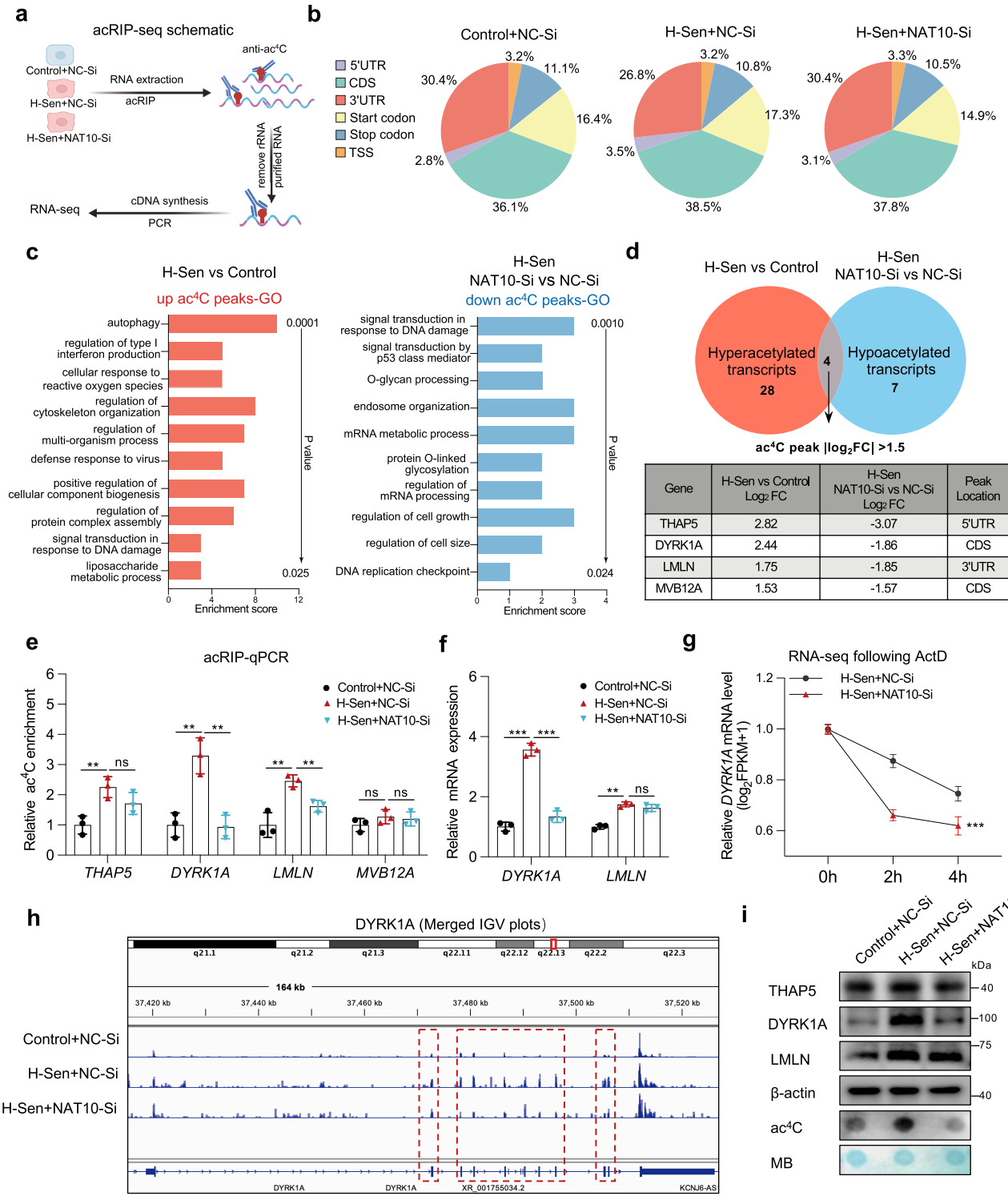

Gene	H-Sen vs Control Log_2 FC	H-Sen NAT10-Si vs NC-Si Log_2 FC	Peak Location
THAP5	2.82	-3.07	5'UTR
DYRK1A	2.44	-1.86	CDS
LMLN	1.75	-1.85	3'UTR
MVB12A	1.53	-1.57	CDS

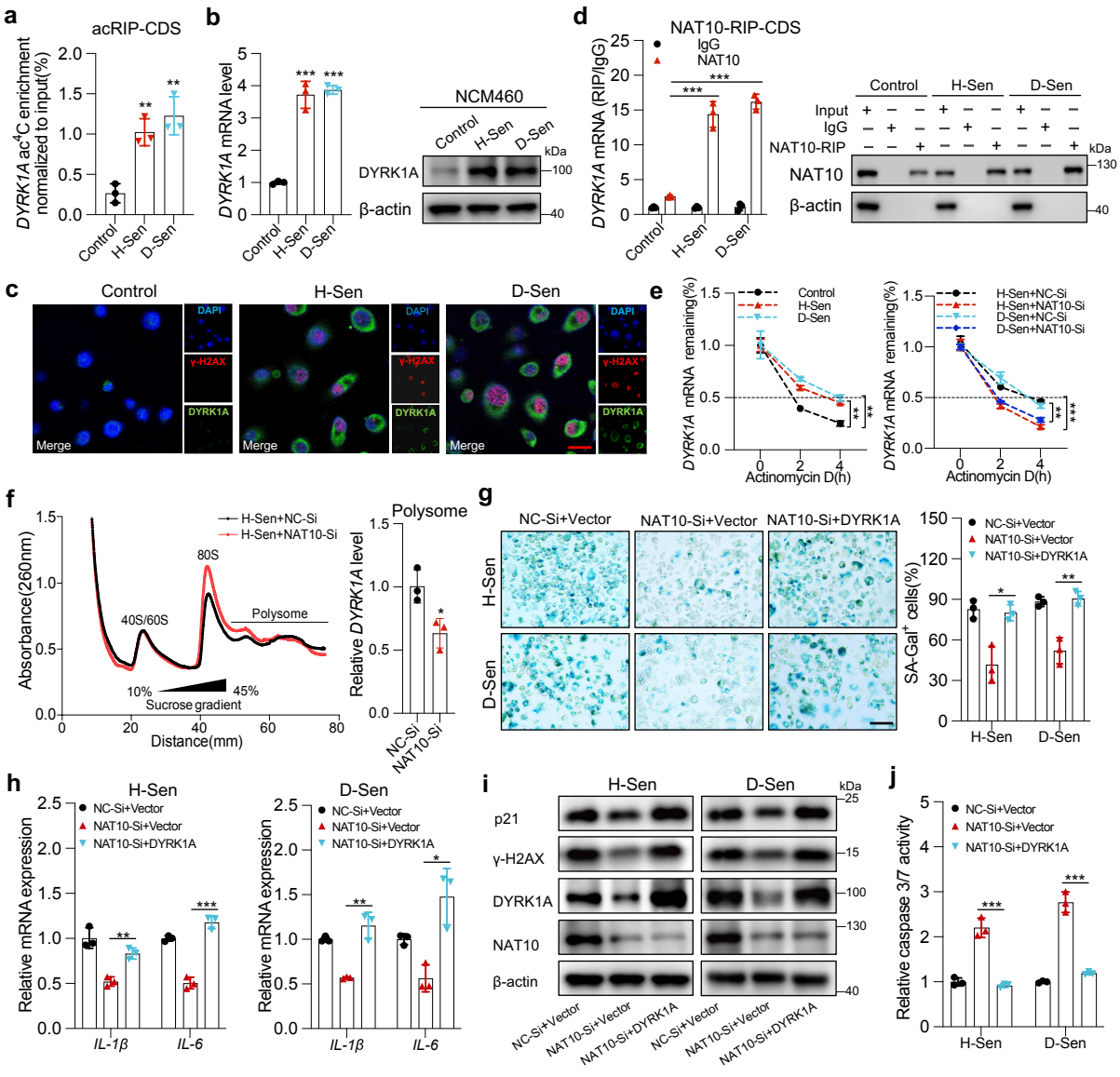
a
acRIP-CDS
DYRK1A ac4C enrichment normalized to input(%)
Control
H-Sen
D-Sen
b
DYRK1A mRNA level
NCM460
DYRK1A
β-actin
kDa
d
NAT10-RIP-CDS
IgG
NAT10
DYRK1A mRNA (RIP/IgG)
Input
NAT10-RIP
NAT10
c
Control
H-Sen
D-Sen
DAPI
γ-H2AX
DYRK1A
Merge
e
DYRK1A mRNA remaining(%)
Actinomycin D(h)
H-Sen+NC-Si
H-Sen+NAT10-Si
D-Sen+NC-Si
D-Sen+NAT10-Si
f
H-Sen+NC-Si
H-Sen+NAT10-Si
80S
40S/60S
Polysome
10%
45%
Sucrose gradient
Absorbance(260nm)
Distance(mm)
Polysome
Relative DYRK1A level
NC-Si
NAT10-Si
g
NC-Si+Vector
NAT10-Si+Vector
NAT10-Si+DYRK1A
H-Sen
D-Sen
SA-Gal+ cells(%)
h
Relative mRNA expression
IL-1β
IL-6
i
p21
γ-H2AX
DYRK1A
NAT10
β-actin
j
Relative caspase 3/7 activity

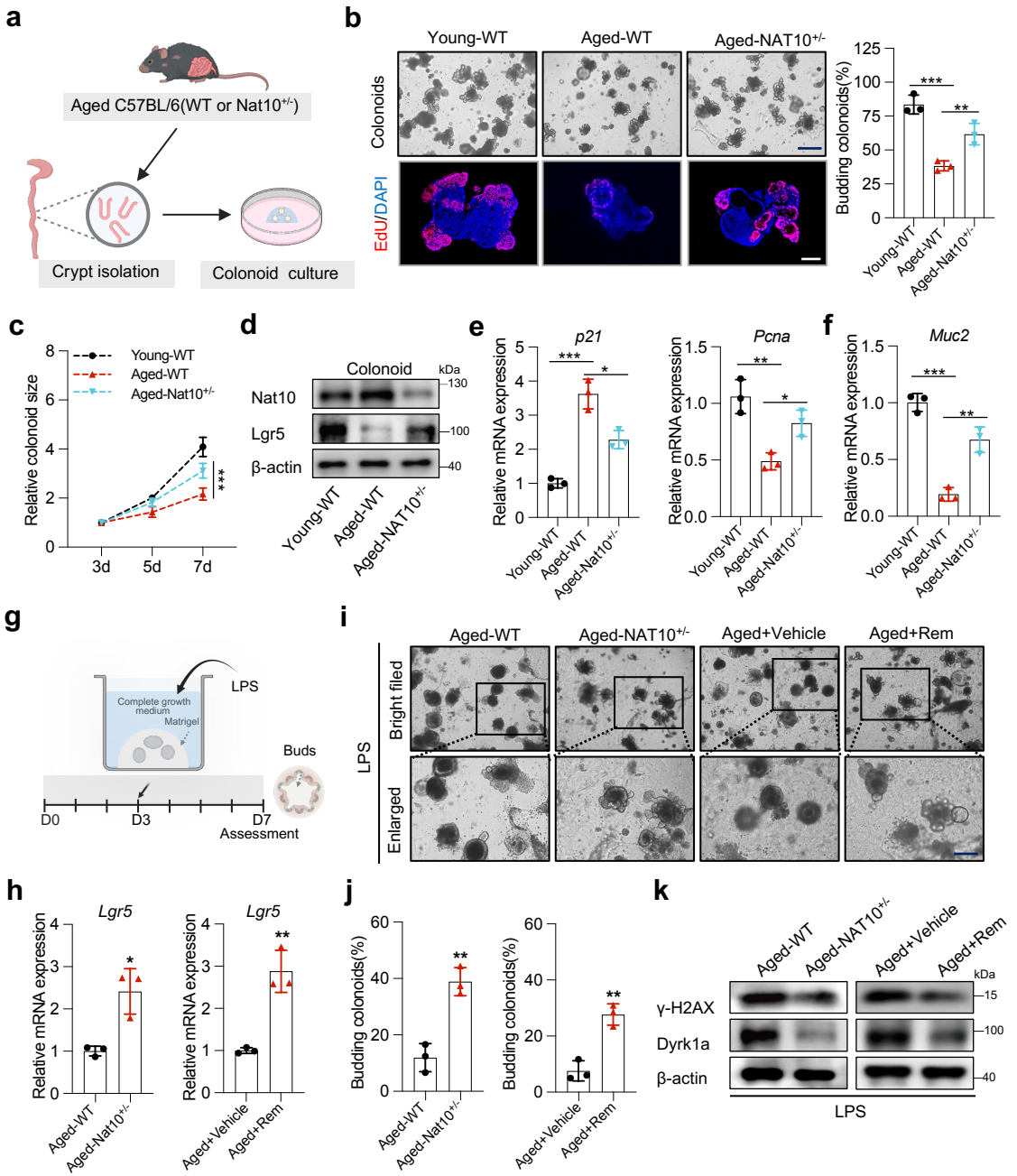
a
Aged C57BL/6(WT or Nat10+/-)
Crypt isolation
Colonoid culture
b
Young-WT
Aged-WT
Aged-NAT10+/-
Colonoids
EdU/DAPI
Budding colonoids(%)
c
Young-WT
Aged-WT
Aged-Nat10+/-
Relative colonoid size
3d
5d
7d
d
Colonoid
kDa
Nat10
Lgr5
β-actin
130
100
40
e
p21
Pcna
Muc2
Relative mRNA expression
f
g
LPS
Complete growth medium
Matrigel
Buds
D0
D3
D7
Assessment
i
Aged-WT
Aged-NAT10+/-
Aged+Vehicle
Aged+Rem
Bright filed
Enlarged
h
Lgr5
j
k
γ-H2AX
Dyrk1a
β-actin

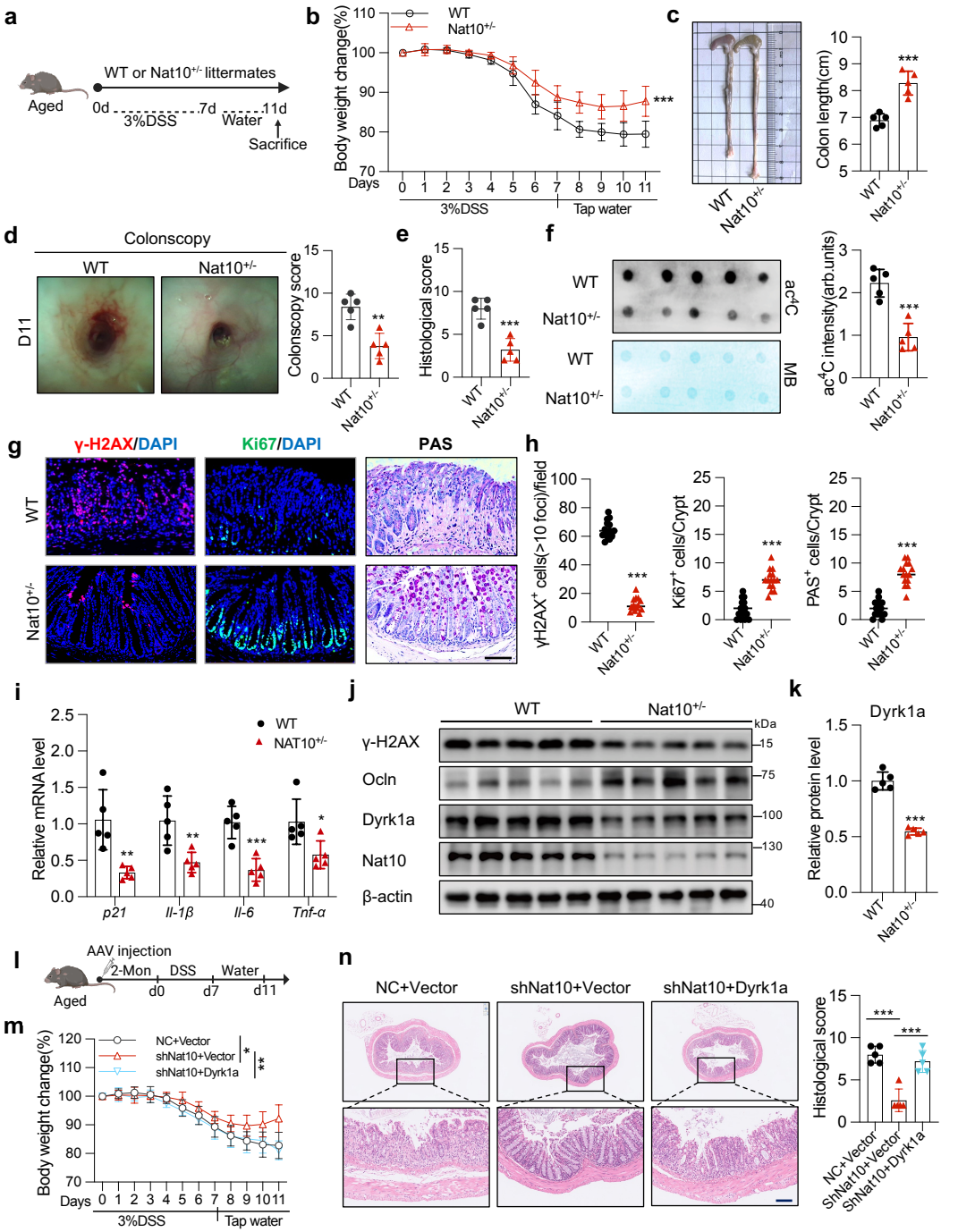
a
Aged
WT or Nat10+/- littermates
0d
7d
11d
3%DSS
Water
Sacrifice
b
Body weight change(%)
WT
Nat10+/-
Days
3%DSS
Tap water
c
Colon length(cm)
WT
Nat10+/-
d
Colonscopy
WT
Nat10+/-
D11
Colonscopy score
e
Histological score
f
WT
Nat10+/-
ac4C
MB
ac4C intensity(arb.units)
g
γ-H2AX/DAPI
Ki67/DAPI
PAS
h
γH2AX+ cells(>10 foci)/field
Ki67+ cells/Crypt
PAS+ cells/Crypt
i
Relative mRNA level
NAT10+/-
p21
Il-1β
Il-6
Tnf-α
j
WT
Nat10+/-
kDa
γ-H2AX
Ocln
Dyrk1a
Nat10
β-actin
k
Dyrk1a
Relative protein level
l
AAV injection
2-Mon
DSS
Water
d0
d7
d11
Aged
m
Body weight change(%)
NC+Vector
shNat10+Vector
shNat10+Dyrk1a
Days
3%DSS
Tap water
n
NC+Vector
shNat10+Vector
shNat10+Dyrk1a
Histological score

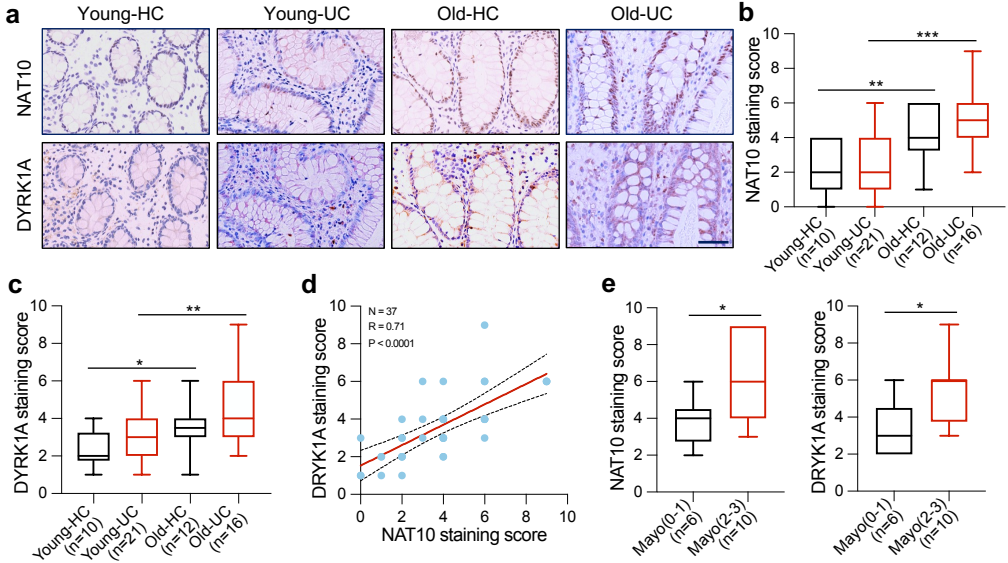
a
Young-HC
Young-UC
Old-HC
Old-UC
NAT10
DYRK1A
b
NAT10 staining score
**
***
Young-HC (n=10)
Young-UC (n=21)
Old-HC (n=12)
Old-UC (n=16)
c
DYRK1A staining score
*
**
Young-HC (n=10)
Young-UC (n=21)
Old-HC (n=12)
Old-UC (n=16)
d
N = 37
R = 0.71
P < 0.0001
DRYK1A staining score
NAT10 staining score
e
NAT10 staining score
*
Mayo(0-1) (n=6)
Mayo(2-3) (n=10)
DRYK1A staining score
*
Mayo(0-1) (n=6)
Mayo(2-3) (n=10)